Inorganic Chemistry
Article

Inorg. Chem. **2009**, *48*, 5685–5696 **5685**
DOI: 10.1021/ic801897k

Redox Chemistry and Electronic Properties of 2,3,5,6-Tetrakis(2-pyridyl)pyrazine-Bridged Diruthenium Complexes Controlled by *N,C,N′*-BisCyclometalated Ligands

Sipke H. Wadman,[†] Remco W. A. Havenith,[‡,¶] František Hartl,[∥] Martin Lutz,[§] Anthony L. Spek,[§] Gerard P. M. van Klink,[†,⊥] and Gerard van Koten*[,†]

[†]*Chemical Biology & Organic Chemistry and* [‡]*Theoretical Chemistry and* [§]*Crystal & Structural Chemistry, Faculty of Science, Utrecht University, Padualaan 8, 3584 CH Utrecht, The Netherlands, and* [∥]*Homogeneous and Supramolecular Catalysis, Van 't Hoff Institute for Molecular Sciences, University of Amsterdam, Nieuwe Achtergracht 166, 1018 WV Amsterdam, The Netherlands.* [⊥]*Present address: DelftChemTech, Faculty of Applied Sciences, Delft University of Technology, Julianalaan 136, 2628 BL Delft, The Netherlands.* [¶]*Also associated with Electronic Structure of Materials, Radboud University Nijmegen, Heyendaalseweg 135, 6525 AJ Nijmegen, The Netherlands*

Received October 5, 2008

To investigate the consequences of cyclometalation for electronic communication in dinuclear ruthenium complexes, a series of 2,3,5,6-tetrakis(2-pyridyl)pyrazine (tppz) bridged diruthenium complexes was prepared and studied. These complexes have a central tppz ligand bridging via nitrogen-to-ruthenium coordination bonds, while each ruthenium atom also binds either a monoanionic, *N,C,N′*-terdentate 2,6-bis(2′-pyridyl)phenyl (R-N^C^N) ligand or a 2,2′:6′,2″-terpyridine (tpy) ligand. The *N,C,N′*-, that is, biscyclometalation, instead of the latter *N,N′,N″*-bonding motif significantly changes the electronic properties of the resulting complexes. Starting from well-known $[\{Ru(tpy)\}_2(\mu\text{-tppz})]^{4+}$ (tpy = 2,2′:2″,6-terpyridine) ($[\mathbf{3}]^{4+}$) as a model compound, the complexes $[\{Ru(R\text{-}N^{\wedge}C^{\wedge}N)\}(\mu\text{-tppz})\{Ru(tpy)\}]^{3+}$ (R-N^C(H)^N = 4-R-1,3-dipyridylbenzene, R = H ($[\mathbf{4a}]^{3+}$), CO_2Me ($[\mathbf{4b}]^{3+}$)), and $[\{Ru(R\text{-}N^{\wedge}C^{\wedge}N)\}_2(\mu\text{-tppz})]^{2+}$, (R = H ($[\mathbf{5a}]^{2+}$), CO_2Me ($[\mathbf{5b}]^{2+}$)) were prepared with one or two *N,C,N′*-cyclometalated terminal ligands. The oxidation and reduction potentials of cyclometalated $[\mathbf{4}]^{3+}$ and $[\mathbf{5}]^{2+}$ are shifted negatively compared to non-cyclometalated $[\mathbf{3}]^{4+}$, the oxidation processes being affected more significantly. Compared to $[\mathbf{3}]^{4+}$, the electronic spectra of $[\mathbf{5}]^{2+}$ display large bathochromic shifts of the main MLCT transitions in the visible spectral region with low-energy absorptions tailing down to the NIR region. One-electron oxidation of $[\mathbf{3}]^{4+}$ and $[\mathbf{5}]^{2+}$ gives rise to low-energy absorption bands. The comproportionation constants and NIR band shape correspond to delocalized Robin-Day class III compounds. Complexes $[\mathbf{4a}]^{3+}$ (R = H) and $[\mathbf{4b}]^{3+}$ (R = CO_2Me) also exhibit strong electronic communication, and notwithstanding the large redox-asymmetry the visible metal-to-ligand charge-transfer absorption is assigned to originate from both metal centers. The potential of the first, ruthenium-based, reversible oxidation process is strongly negatively shifted. On the contrary, the second oxidation is irreversible and cyclometalated ligand-based. Upon one-electron oxidation, a weak and low-energy absorption arises.

Introduction

Polynuclear metal complexes exhibiting intermetallic electronic coupling in mixed valence states have been an actively studied class of coordination compounds for decades.[1−7] This permanent and recently strongly growing interest stems from the need to intimately understand factors that influence the degree and mechanism of electronic communication and its implications, for example, for optical electron transfer. Possible applications are abundant, ranging from molecular electronics,[8−11] bioinorganic chemistry,[12,13] to aerospace.[14]

*To whom correspondence should be addressed. E-mail: g.vankoten@uu.nl.

(1) Giuffrida, G.; Campagna, S. *Coord. Chem. Rev.* **1994**, *135*, 517–531.
(2) Kaim, W.; Sarkar, B. *Coord. Chem. Rev.* **2007**, *251*, 584–594.
(3) Demadis, K. D.; Hartshorn, C. M.; Meyer, T. J. *Chem. Rev.* **2001**, *101*, 2655–2685.
(4) Baranoff, E.; Collin, J.-P.; Flamigni, L.; Sauvage, J.-P. *Chem. Soc. Rev.* **2004**, *33*, 147–155.
(5) De Cola, L.; Belser, P. *Coord. Chem. Rev.* **1998**, *177*, 301–346.
(6) Vos, J. G.; Kelly, J. M. *Dalton Trans.* **2006**, 4869–4883.
(7) D'Alessandro, D. M.; Keene, F. R. *Chem. Rev.* **2006**, *106*, 2270–2298.
(8) Davis, W. B.; Svec, W. A.; Ratner, M. A.; Wasielewski, M. R. *Nature* **1998**, *396*, 60–63.
(9) Flores-Torres, S.; Hutchison, G. R.; Soltzberg, L. J.; Abruna, H. D. *J. Am. Chem. Soc.* **2006**, *128*, 1513–1522.
(10) Fantacci, S.; De Angelis, F.; Wang, J. J.; Bernhard, S.; Selloni, A. *J. Am. Chem. Soc.* **2004**, *126*, 9715–9723.
(11) De Cola, L. *Top. Curr. Chem.* Springer: Berlin, 2005; Vol. 257.
(12) Solomon, E. I.; Brunold, T. C.; Davis, M. I.; Kemsley, J. N.; Lee, S.-K.; Lehnert, N.; Neese, F.; Skulan, A. J.; Yang, Y.-S.; Zhou, J. *Chem. Rev.* **2000**, *100*, 235–349.
(13) Wei, P.-P.; Skulan Andrew, J.; Mitic, N.; Yang, Y.-S.; Saleh, L.; Bollinger, J. M.Jr.; Solomon, E. I. *J. Am. Chem. Soc.* **2004**, *126*, 3777–3788.
(14) Chandrasekhar, P.; Zay, B. J.; Birur, G. C.; Rawal, S.; Pierson, E. A.; Kauder, L.; Swanson, T. *Adv. Funct. Mater.* **2002**, *12*, 95–103.

Published on Web 06/10/2009

The archetypical example of a dimetallic complex exhibiting strong intermetallic coupling is the pyrazine-bridged diruthenium Creutz-Taube complex $[\{Ru(NH_3)_5\}_2(\mu\text{-pyrazine})]^{5+}$.[15−17] The extent of the effective electronic communication between the metal centers is strongly dependent on the nature of the bridging ligand. Several other factors exert an influence on the coupling, such as the nature of the metal centers and the ancillary ligands. As a result many examples of diruthenium complexes exist, with a variety of bridging ligands, coordinated in mono-, bi-, or tridentate fashion.[2] For its resemblance of the pyrazine bridging ligand in the Creutz-Taube complex, 2,3,5,6-tetrakis(2-pyridyl)pyrazine (tppz)[18] has been used in several studies.[9,10,19−29] The bis(tridentate) coordination of tppz facilitates purification and analysis of the resulting complexes, since no diastereomers or enantiomers are formed, as is the case with diruthenium complexes containing bis(bidentate) bridging ligands. Although tppz is non-planar when coordinated in bridging mode, it supports significant electronic communication.

We have recently demonstrated that the class of cyclometalated bridging ligands which contain a covalent bond between the metal center and a formally anionic carbon donor atom, are of particular interest.[33,34] Complexes such as $[(Ru(ttpy))_2(\mu\text{-tpbp})](PF_6)_2$ (ttpy = 4′-tolyl-2,2′:6′,2″-terpyridine; $tpbpH_2$ = 3,3′,5,5′-tetrakis(2″-pyridyl)biphenyl),[30−32] $[(Ru(tpy))_2(\mu\text{-}L^1)](PF_6)_2$ (tpy = 2,2′:6′,2″-terpyridine; L^1H_2 = 3,3′,5,5′-tetrakis[(dimethylamino)methyl]biphenyl),[33,34] and its phosphorus congener $[(Ru(tpy))_2(\mu\text{-}L^2)](PF_6)_2$ (L^2H_2 = 3,3′,5,5′-tetrakis[(diphenylphosphino)methyl]biphenyl)[35] exhibit enhanced metal−metal interaction, compared to their non-metalated analogues. The covalent carbon-to-metal bond in these complexes results in a significant contribution of the ligand to the highest occupied molecular orbital (HOMO) of the complexes. This contribution can in some cases be pronounced to such an extent that the NIR transitions observed in the mixed valence state may be better described as metal-to-ligand charge transfer (MLCT) rather than intervalence charge transfer (IVCT).[35]

To address the influence of the strong σ-donor on the electronic properties of dimetallic ruthenium complexes we focused our attention on complexes containing the all-nitrogen donor atom bridging ligand tppz and introduced cyclometalating peripheral ligands. With the well-defined and stable reference complex $[(Ru(tpy))_2(\mu\text{-tppz})](PF_6)_4$, $[\mathbf{3}]^{4+}$ in mind, we prepared the novel species $[\{Ru(R\text{-}N^\wedge C^\wedge N)\}_2(\mu\text{-tppz})](PF_6)_2$ (R-N^C(H)^N = 4-R-2,6-dipyridylbenzene, R = H ($[\mathbf{5a}]^{2+}$), CO_2Me ($[\mathbf{5b}]^{2+}$)), Scheme 1. We show that cyclometalation of the peripheral ligands significantly changes the electronic properties of the ruthenium center, while leaving the overall geometry of the complex intact. As the generation of an electronic gradient by optical excitation can be beneficial for the application of electron transfer processes in redox-unsymmetrical dimetallic compounds,[36−39] we also prepared the intermediate complexes $[\mathbf{4a}]^{3+}$ and $[\mathbf{4b}]^{3+}$, being cyclometalated at one ruthenium site only. TD-DFT calculations are used as an indicative tool to rationalize the spectroscopic and spectroelectrochemical investigations of the series.

Results

Synthesis. The previously reported complexes $[\mathbf{1}]^{2+}$ and $[\mathbf{3}]^{4+}$ were prepared stepwise starting from uncoordinated 2,3,5,6-tetrakis(2-pyridyl)pyrazine (tppz), Scheme 1. Their NMR spectra, electronic absorption spectra, and redox data agree well with those previously reported in literature.[27,28,36]

The ligands 1,3-di(2-pyridyl)benzene, H−N^C(H)^N, and methyl 3,5-di(2-pyridyl)benzoate, MeO_2C−N^C(H)^N, were prepared according to literature procedures.[40,41] For the cyclometalated complexes $[\mathbf{2}]^{+}$, $[\mathbf{4a}]^{3+}$, $[\mathbf{4b}]^{3+}$, $[\mathbf{5a}]^{2+}$, and $[\mathbf{5b}]^{2+}$ we adopted a stepwise synthetic procedure starting from tppz. From the work of Pfeffer et al.[42] it is known that the dimer $[\{RuCl_2(\eta^6\text{-}C_6H_6)\}_2(\mu\text{-}Cl)_2]$ reacts with 2-phenylpyridine, C(H)^N, in MeCN in the presence of NaOH and KPF_6 to yield the corresponding bidentate *C,N*-cyclometalated complex, where the π-bound benzene can be replaced by MeCN upon irradiation. The product can be further reacted with 2,2′-bipyridine (bpy) to yield the corresponding complexes $[Ru(C^\wedge N)(bpy)(MeCN)_2](PF_6)$.[43,44]

(15) Creutz, C.; Taube, H. *J. Am. Chem. Soc.* **1969**, *91*, 3988–3989.
(16) Creutz, C.; Taube, H. *J. Am. Chem. Soc.* **1973**, *95*, 1086–1094.
(17) Fuerholz, U.; Joss, S.; Buergi, H. B.; Ludi, A. *Inorg. Chem.* **1985**, *24*, 943–948.
(18) Goodwin, H. A.; Lions, F. *J. Am. Chem. Soc.* **1959**, *81*, 6415–6422.
(19) Jones, S. W.; Vrana, L. M.; Brewer, K. J. *J. Organomet. Chem.* **1998**, *554*, 29–40.
(20) Ghumaan, S.; Sarkar, B.; Chanda, N.; Sieger, M.; Fiedler, J.; Kaim, W.; Lahiri, G. K. *Inorg. Chem.* **2006**, *45*, 7955–7961.
(21) Dattelbaum, D. M.; Hartshorn, C. M.; Meyer, T. J. *J. Am. Chem. Soc.* **2002**, *124*, 4938–4939.
(22) Chanda, N.; Laye, R. H.; Chakraborty, S.; Paul, R. L.; Jeffrey, J. C.; Ward, M. D.; Lahiri, G. K. *J. Chem. Soc., Dalton Trans.* **2002**, 3496–3504.
(23) Chanda, N.; Sarkar, B.; Fiedler, J.; Kaim, W.; Lahiri, G. K. *Dalton Trans.* **2003**, 3550–3555.
(24) Chanda, N.; Sarkar, B.; Kar, S.; Fiedler, J.; Kaim, W.; Lahiri, G. K. *Inorg. Chem.* **2004**, *43*, 5128–5133.
(25) Hartshorn, C. M.; Daire, N.; Tondreau, V.; Loeb, B.; Meyer, T. J.; White, P. S. *Inorg. Chem.* **1999**, *38*, 3200–3206.
(26) Vogler, L. M.; Brewer, K. J. *Inorg. Chem.* **1996**, *35*, 818–824.
(27) Thummel, R. P.; Chirayil, S. *Inorg. Chim. Acta* **1988**, *154*, 77–81.
(28) Arana, C. R.; Abruna, H. D. *Inorg. Chem.* **1993**, *32*, 194–203.
(29) Zhao, S.; Arachchige, S. M.; Slebodnick, C.; Brewer, K. J. *Inorg. Chem.* **2008**, *47*, 6144–6152.
(30) Beley, M.; Collin, J. P.; Louis, R.; Metz, B.; Sauvage, J.-P. *J. Am. Chem. Soc.* **1991**, *113*, 8521–8522.
(31) Beley, M.; Collin, J. P.; Sauvage, J.-P. *Inorg. Chem.* **1993**, *32*, 4539–4543.
(32) Patoux, C.; Launay, J.-P.; Beley, M.; Chodorowski-Kimmes, S.; Collin, J. P.; James, S.; Sauvage, J.-P. *J. Am. Chem. Soc.* **1998**, *120*, 3717–3725.
(33) Steenwinkel, P.; Grove, D. M.; Veldman, N.; Spek, A. L.; van Koten, G. *Organometallics* **1998**, *17*, 5647–5655.
(34) Sutter, J. P.; Grove, D. M.; Beley, M.; Collin, J. P.; Veldman, N.; Spek, A. L.; Sauvage, J.-P.; van Koten, G. *Angew. Chem., Int. Ed. Engl.* **1994**, *33*, 1282–1285.
(35) Gagliardo, M.; Amijs, C. H. M.; Lutz, M.; Spek, A. L.; Havenith, R. W. A.; Hartl, F.; van Klink, G. P. M.; van Koten, G. *Inorg. Chem.* **2007**, *46*, 11133–11144.
(36) Vogler, L. M.; Scott, B.; Brewer, K. J. *Inorg. Chem.* **1993**, *32*, 898–903.
(37) Lee, J. D.; Vrana, L. M.; Bullock, E. R.; Brewer, K. J. *Inorg. Chem.* **1998**, *37*, 3575–3580.
(38) Börgstrom, M.; Ott, S.; Lomoth, R.; Bergquist, J.; Hammarström, L.; Johansson, O. *Inorg. Chem.* **2006**, *45*, 4820–4829.
(39) Ott, S.; Borgström, M.; Hammarström, L.; Johansson, O. *Dalton Trans.* **2006**, 1434–1443.
(40) Sindkhedkar, M. D.; Mulla, H. R.; Wurth, M. A.; Cammers-Goodwin, A. *Tetrahedron* **2001**, *57*, 2991–2996.
(41) Neve, F.; Crispini, A.; Di Pietro, C.; Campagna, S. *Organometallics* **2002**, *21*, 3511–3518.
(42) Fernandez, S.; Pfeffer, M.; Ritleng, V.; Sirlin, C. *Organometallics* **1999**, *18*, 2390–2394.
(43) Le Lagadec, R.; Rubio, L.; Alexandrova, L.; Toscano, R. A.; Ivanova, E. V.; Meskys, R.; Laurinavicius, V.; Pfeffer, M.; Ryabov, A. D. *J. Organomet. Chem.* **2004**, *689*, 4820–4832.
(44) Ryabov, A. D.; Sukharev, V. S.; Alexandrova, L.; Le Lagadec, R.; Pfeffer, M. *Inorg. Chem.* **2001**, *40*, 6529–6532.

Scheme 1. Synthesis and NMR Numbering of $[\mathbf{1}]^{2+}-[\mathbf{5}]^{2+}$ [a]

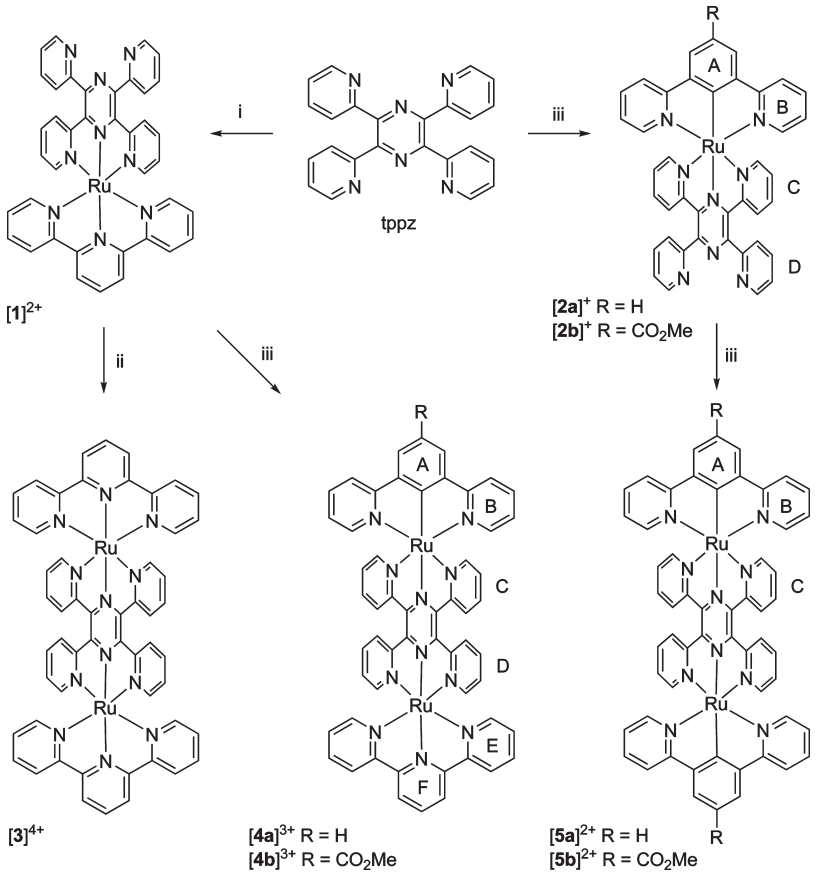

[a] (i) $[RuCl_3(tpy)]$, NEt_3, H_2O/EtOH, reflux; (ii) $[RuCl_3(tpy)]$, ethylene glycol, reflux; (iii) $[Ru(R\text{-}N\hat{}C\hat{}N)(MeCN)_3](PF_6)$, DMF, reflux.

Scheme 2. Synthesis of $[\mathbf{2a}]^+$ and $[\mathbf{2b}]^+$ [a]

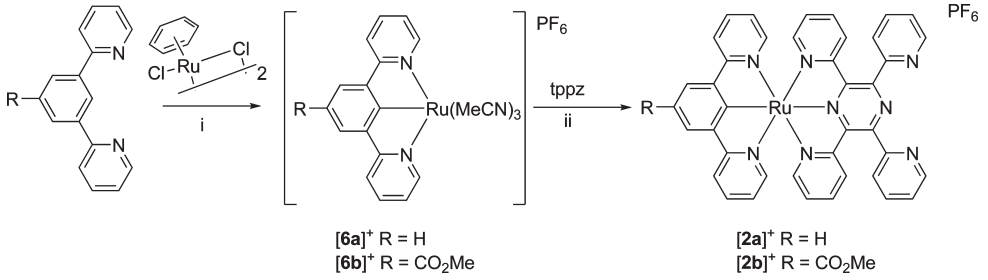

[a] (i) NaOH, KPF_6, MeCN, 45 °C, 15 h; (ii) DMF, reflux 3 h.

Indeed, $[\{RuCl_2(\eta^6\text{-}C_6H_6)\}_2(\mu\text{-}Cl)_2]$ reacts with $MeO_2C-N\hat{}C(H)\hat{}N$ in MeCN solution in the presence of NaOH and KPF_6 to yield a tridentate coordinated complex, $[\mathbf{6b}]^+$, Scheme 2. The ^1H NMR spectrum in MeCN shows the five aromatic resonances expected for the symmetrically coordinated ligand. In $[\mathbf{6b}]^+$ the π-bound benzene is already replaced by MeCN, without the need for irradiation. In the MeCN solution a minor congener, $[\mathbf{7b}]^+$, is present which shows the same high degree of symmetry as $[\mathbf{6b}]^+$. However, in DCM $[\mathbf{7b}]^+$ is the major species and corresponds to the loss of one MeCN ligand as judged from the appearance of one molar equivalent of free MeCN in solution. Both $[\mathbf{6b}]^+$ and $[\mathbf{7b}]^+$ can be reacted with either tppz, $[\mathbf{1}]^{2+}$ or $[\mathbf{2b}]^+$ to yield the corresponding complexes $[\mathbf{2b}]^+$, $[\mathbf{4b}]^{3+}$, and $[\mathbf{5b}]^{2+}$ in moderate yields. Slow distillation of Et_2O into a MeCN solution of $[\mathbf{6b}]^+$ yielded crystals suitable for X-ray diffraction analysis (Figure 1). The molecular structure shows the presence of three coordinated MeCN molecules, vide infra.

When $[\{RuCl_2(\eta^6\text{-}C_6H_6)\}_2(\mu\text{-}Cl)_2]$ is reacted with the parent $N\hat{}C(H)\hat{}N$ ligand, a complex reaction mixture is obtained, as evidenced by ^1H NMR spectroscopy. Although the exact composition of this mixture remained largely unknown, it contained most likely species in which the $N\hat{}C\hat{}N$ ligand is bound as bidentate *C,N*-cyclometalated at either the 1- or 3-positions of the phenyl ring, in addition to the desired tridentate *N,C,N′*-coordinated products $[\mathbf{6a}]^+$ and $[\mathbf{7a}]^+$. When this mixture is subsequently reacted with either tppz or $[\mathbf{1}]^{2+}$, the mono- and diruthenium complexes $[\mathbf{2a}]^+$ and $[\mathbf{4a}]^{3+}$, respectively,

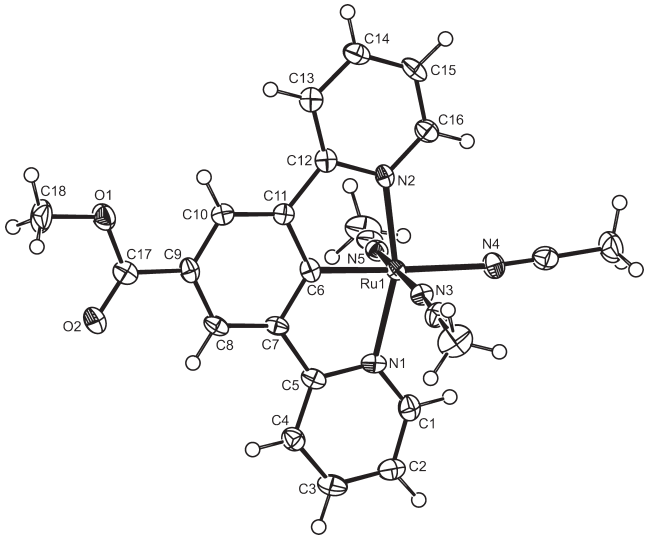

Figure 1. Displacement ellipsoid plot (50% probability level) of the $[Ru(MeO_2C{-}N^C^N)(MeCN)_3]$ cation $[\mathbf{6b}]^+$. The disordered PF_6^- counterion has been omitted for clarity.

are obtained in varying yields. The diruthenium complex $[\mathbf{5a}]^{2+}$ was prepared by a microwave-assisted reaction of $[(RuCl_3)_2(\mu\text{-tppz})]$ with N^C(H)^N in ethylene glycol in the presence of *N*-methylmorpholine as sacrificial reductant.

Molecular Structures in the Solid State. The molecular structure of $[Ru(MeO_2C{-}N^C^N)(MeCN)_3](PF_6)$ is depicted in Figure 1, and selected bond lengths and angles are given in Table 1. The structure shows the expected tridentate-coordinated $MeO_2C{-}N^C(H)^N$ ligand, and three coordinated MeCN molecules in a *mer*-arrangement. The outer pyridyl nitrogen-to-ruthenium bonds of 2.092(5) and 2.091(5) Å, respectively, are in the range expected for tridentate *N*,*N*′,*N*″-coordinated ligands (2.073 ± 0.023 Å).[45] The N−Ru−N bite angle of 159.5(2)° is also in the range observed for tridentate *N*,*N*′,*N*″-bonded ligands (158.3 ± 1.05°).[45] The ruthenium-to-carbon bond (1.925(6) Å) is relatively short compared to the bidentate *C*,*N*-cyclometalated complex $[Ru(C^N)(MeCN)_4](PF_6)$ (2.014(6) Å),[46] and the tridentate *N*,*C*,*N*′-cyclometalated bis(*o*-diamine) complex $[RuI(2,6\text{-}(Me_2NCH_2)_2C_6H_3)(PPh_3)]$ (1.967(2) Å).[47] The axially coordinated MeCN molecules have nitrogen-to-ruthenium bond distances of 2.023(5) Å and 2.007(5) Å, close to the average value for this bond found in the Cambridge Structural Database (2.064 Å, SD = 0.051 Å).[45] However, the meridional MeCN ligand exhibits a much longer ruthenium-to-nitrogen distance of 2.164(5) Å. The same effect is observed in $[Ru(C^N)(MeCN)_4](PF_6)$, with a nitrogen-to-ruthenium bond length of 2.148(6)−2.153(6) Å for the MeCN ligand *trans* to the anionic *ipso* carbon. The strong σ-donor properties

Table 1. Selected Bond Lengths (Å) and Angles (deg) for $[Ru(MeO_2C{-}N^C^N)(MeCN)_3](PF_6)$, $[\mathbf{6b}](PF_6)$

Ru1−C6	1.925(6)	Ru1−N3	2.023(5)	N1−Ru1−N2	159.5(2)
Ru1−N1	2.092(5)	Ru1−N4	2.164(5)	N3−Ru1−N5	174.6(2)
Ru1−N2	2.091(5)	Ru1−N5	2.007(5)	C6−Ru1−N4	176.2(2)

of the monoanionic carbon center result in a weaker bonding of the meridional MeCN ligand, which in the present case results in the reversible loss of this ligand in dichloromethane solution, that is, in the formation of $[\mathbf{7b}]^+$.

^{1}H NMR spectroscopy. The ^{1}H NMR spectra of $[\mathbf{1}]^{2+}$−$[\mathbf{5}]^{2+}$ are consistent with the structures as proposed in Scheme 1. As a representative example the ^{1}H NMR spectrum and two-dimensional COSY spectrum of $[\mathbf{4a}]^{3+}$ are displayed in Supporting Information, Figure S1, showing the expected 20 unique resonances. All resonances have been assigned unequivocally with the aid of COSY and NOESY experiments. In $[\mathbf{4a}]^{3+}$ the resonances of the protons on terminal H−N^C^N and tpy ligands are very dissimilar. The resonance patterns for $[\mathbf{3}]^{4+}$ and $[\mathbf{5a}]^{2+}$ are comparable with those observed for the non-metalated and cyclometalated sides of $[\mathbf{4a}]^{3+}$, respectively. The tpy protons F3,5 and F4 are found at 8.89 and 8.58 ppm, respectively, which is normal for $[Ru(tpy)_2]$ type complexes. The corresponding H−N^C^N protons A3,5 and A4, on the other hand, are found at 8.41 and 7.66 ppm, respectively, being strongly upfield shifted. Similarly, the resonance of B5 on the H−N^C^N ligand is found at 6.80 ppm, being shifted upfield compared to the corresponding resonance of E5 in the tpy ligand found at 7.35 ppm. The upfield shift of the resonances in H−N^C^N compared to the tpy ligand reflects the increased electron density on the cyclometalated ligand. To a lesser extent differences are observed between the pyridyl rings of the bridging tppz ligand when coordinated to the cyclometalated ruthenium center or the non-metalated center. While the resonance of C3 is shifted downfield compared to D3, the other resonances are shifted upfield. Similar but smaller differences between the chemical shifts of the protons on the cyclometalated and non-metalated ruthenium moiety are observed in $[\mathbf{4b}]^{3+}$. The ^{13}C resonance of the *ipso* carbon nucleus is found at 227.4 ppm for $[\mathbf{4b}]^{3+}$, and 217.6 ppm for $[\mathbf{4a}]^{3+}$.

Electrochemistry. Electrochemical data are collected in Table 2, and representative cyclic voltammograms are shown in Figure 2. In polypyridine complexes of ruthenium(II), the anodic processes are predominantly ruthenium-based, while the cathodic processes are ligand-based.[48−50] The anodic process is negatively shifted by 760 and 640 mV for $[\mathbf{2a}]^+$ and $[\mathbf{2b}]^+$ compared to $[\mathbf{1}]^{2+}$, respectively. Similar potential shifts are reported for various bis(terpyridine)-type *N*,*C*,*N*′- and *C*,*N*,*N*′-cyclometalated ruthenium complexes.[32,51,52] Somewhat larger shifts are observed for $[\mathbf{5a}]^{2+}$ and $[\mathbf{5b}]^{2+}$, namely, 810 and 700 mV compared to $[\mathbf{3}]^{4+}$, respectively.

(45) Allen, F. H.; Davies, J. E.; Galloy, J. J.; Johnson, O.; Kennard, O.; Macrae, C. F.; Mitchell, E. M.; Mitchell, G. F.; Smith, J. M.; Watson, D. G. *J. Chem. Inf. Comput. Sci.* **1991**, *31*, 187–204.
(46) Ryabov, A. D.; Le Lagadec, R.; Estevez, H.; Toscano, R. A.; Hernandez, S.; Alexandrova, L.; Kurova, V. S.; Fischer, A.; Sirlin, C.; Pfeffer, M. *Inorg. Chem.* **2005**, *44*, 1626–1634.
(47) Sutter, J. P.; James, S. L.; Steenwinkel, P.; Karlen, T.; Grove, D. M.; Veldman, N.; Smeets, W. J. J.; Spek, A. L.; van Koten, G. *Organometallics* **1996**, *15*, 941–948.
(48) Campagna, S.; Puntoriero, F.; Nastasi, F.; Bergamini, G.; Balzani, V. *Top. Curr. Chem.* **2007**, *280*, 117–214.
(49) Balzani, V.; Bergamini, G.; Campagna, S.; Puntoriero, F. *Top. Curr. Chem.* **2007**, *280*, 1–36.
(50) Juris, A.; Balzani, V.; Barigelletti, F.; Campagna, S.; Belser, P.; Von Zelewsky, A. *Coord. Chem. Rev.* **1988**, *84*, 85–277.
(51) Wadman, S. H.; Kroon, J. M.; Bakker, K.; Lutz, M.; Spek, A. L.; van Klink, G. P. M.; van Koten, G. *Chem. Commun.* **2007**, 1907–1909.
(52) Barigelletti, F.; Ventura, B.; Collin, J. P.; Kayhanian, R.; Gavina, P.; Sauvage, J.-P. *Eur. J. Inorg. Chem.* **2000**, 113–119.

Table 2. Electrochemical Data[a] for $[\mathbf{1}]^{2+}$–$[\mathbf{5}]^{2+}$ and Relevant tppz-Bridged Complexes from the Literature

	$E_{1/2}$ (V) (ΔE_p (mV))					
compound	Ru'^{II}/Ru'^{III}	Ru^{II}/Ru^{III}	tppz/tppz$^{\bullet -}$	tppz$^{\bullet -}$/tppz^{2-}	tpy/tpy$^{\bullet -}$	$\Delta E_{1/2}$(ox)[b]
$[\mathbf{1}]^{2+}$		1.02 (65)	−1.36 (60)		−1.79 (65)	
$[\mathbf{2a}]^{+}$		0.26 (60)	−1.59 (60)			
$[\mathbf{2b}]^{+}$		0.38 (65)	−1.56 (60)			
$[\mathbf{3}]^{4+}$	1.35 (85)	1.03 (75)	−0.76 (60)	−1.25 (60)	−1.83 (115)	320
$[\mathbf{4a}]^{3+}$[c]	1.19[d]	0.38 (60)	−0.96 (60)	−1.44 (65)	−1.85 (65)	
$[\mathbf{4b}]^{3+}$	1.21[d]	0.49 (65)	−0.93 (60)	−1.41 (60)	−1.84 (70)	
$[\mathbf{5a}]^{2+}$	0.49 (60)	0.21 (55)	−1.14 (60)	−1.61 (60)		280
$[\mathbf{5b}]^{2+}$	0.66 (60)	0.33 (55)	−1.08 (55)	−1.56 (60)		330
$[\{RuCl(L)\}_2(\mu\text{-tppz})]$[e,f]	0.34 (85)	0.08 (90)	−1.19 (70)	−1.72 (95)		260
$[\{RuCl(bpy)\}_2(\mu\text{-tppz})]^{2+}$ [f,g]	0.90	0.61	−0.95	−1.45		290

[a] Data collected in MeCN with $[n\text{-}Bu_4N]PF_6$ as supporting electrolyte at 100 mV/s; potentials reported relative vs ferrocene/ferrocenium (Fc/Fc^+) used as internal reference. [b] Separation between the two successive Ru^{II}/Ru^{III} couples ($E_{1/2}$(ox2) − $E_{1/2}$(ox1)). [c] Third, chemically irreversible anodic wave observed at $E_{p,a}$ = 1.45 V. [d] Chemically irreversible, $E_{p,a}$ reported. Localized probably on the orthometalated ligand. [e] L = 2-(2-pyridyl)-benzimidazolate.[24] [f] Reported in the literature against SCE, the Fc/Fc^+ couple found at 0.35 V vs SCE.[53,54] [g] bpy = 2,2′-bipyridine.[25]

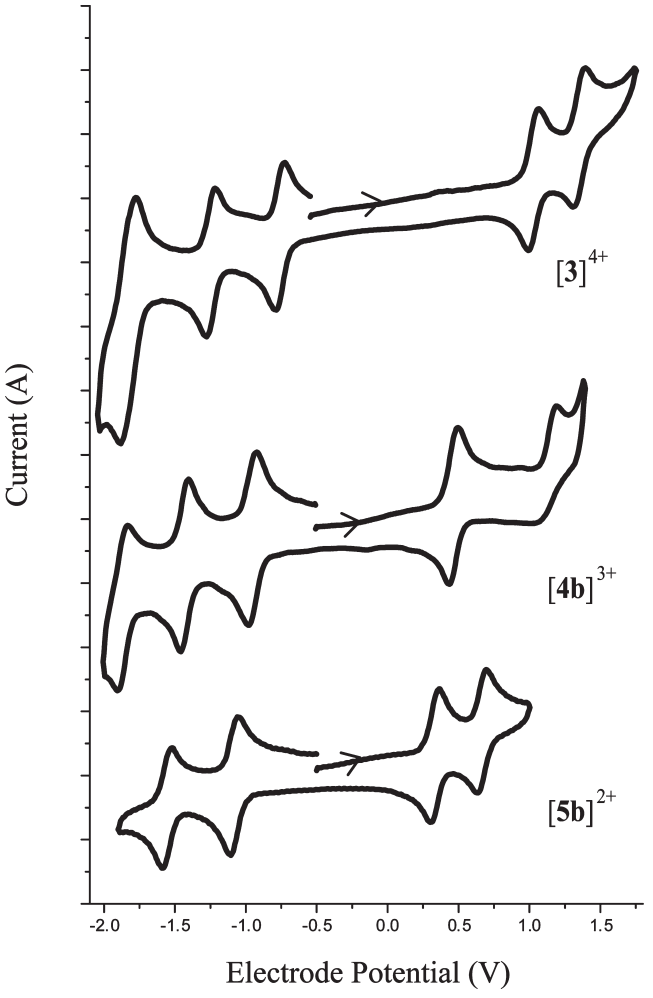

Figure 2. Cyclic voltammograms of complexes $[\mathbf{3}]^{4+}$, $[\mathbf{4b}]^{3+}$, and $[\mathbf{5b}]^{2+}$. Experimental parameters are given in Table 2.

The electrochemistry of $[\mathbf{3}]^{4+}$ has been reported elsewhere.[21,28] The separation of the oxidation waves ($\Delta E_{1/2}$(ox) = $E_{1/2}$(ox2) − $E_{1/2}$(ox1)) is ascribed to the strong electronic communication between the two ruthenium centers across the tppz bridging ligand.[21,28] The value of $\Delta E_{1/2}$(ox) = 0.320 V in the present study agrees with the reported value of 310 mV that was also obtained for $[\mathbf{3}]^{4+}$ in MeCN.[28] The present value corresponds to a comproportionation constant $K_c = 2.6 \times 10^5$ for $[\mathbf{3}]^{5+}$ as calculated from $RT \ln K_c = nF(\Delta E_{1/2}(ox))$. For $[\mathbf{5a}]^{2+}$ and $[\mathbf{5b}]^{2+}$ the $\Delta E_{1/2}$(ox) values of 0.28 and 0.33 V, respectively, correspond to $K_c = 5.4 \times 10^4$ for $[\mathbf{5a}]^{3+}$ and $K_c = 3.8 \times 10^5$, for $[\mathbf{5b}]^{3+}$.

The redox-unsymmetrical complexes $[\mathbf{4a}]^{3+}$ (R = H) and $[\mathbf{4b}]^{3+}$ (R = CO_2Me) show a reversible initial one-electron oxidation process assigned to the cyclometalated Ru^{II}/Ru^{III} couple. The anodic process is negatively shifted by 650 and 540 mV for $[\mathbf{4a}]^{3+}$ and $[\mathbf{4b}]^{3+}$, respectively, compared to $[\mathbf{3}]^{4+}$. The second oxidation step is chemically irreversible. The difference between the anodic electrode potentials reflects the redox-asymmetry between the two ruthenium centers.

The bridging tppz ligand is a well-known redox active center, being reduced at less negative potentials because of its strong π-acidity. In dimetallic complexes tppz usually accommodates two electrons before the terminal ligands are reduced.[22−25,28] UV−vis−NIR spectroelectrochemical measurements with complexes $[\mathbf{3}]^{4+}$ and $[\mathbf{4a}]^{3+}$ were performed at room temperature using an optically transparent thin-layer electrochemical (OTTLE) cell[55] to obtain accurate reference electronic absorption spectra of the complexes in several oxidation states. Electrochemical reduction experiments were performed in THF:MeCN 3:1 (v/v) to ensure solubility of the species in the various oxidation states. The results support the assignment of the reduction processes as in Table 2. In the course of the electrolyses, and stepwise chemical oxidation (vide infra), sharp isosbestic points are maintained. Upon the reversible one-electron reduction of complexes $[\mathbf{3}]^{4+}$ and $[\mathbf{4a}]^{3+}$, a weak low-energy band appears around 1100 nm, typical for the radical anion of bridging tppz.[20,23,24] Upon further reduction to $[\mathbf{3}]^{2+}$ and $[\mathbf{4a}]^{+}$, this band is replaced by bands typical for the bridging $tppz^{2-}$ chromophore.[20,24] Further two-electron reduction of $[\mathbf{3}]^{2+}$ and one-electron reduction of $[\mathbf{4a}]^{+}$ result in the appearance of bands associated with the radical anion of tpy.[56] Reduction of $[\mathbf{5a}]^{2+}$ was irreversible under the experimental conditions.

(53) Kolthoff, I. M.; Thomas, F. G. *J. Phys. Chem.* **1965**, *69*, 3049–3058.
(54) Pavlishchuk, V. V.; Addison, A. W. *Inorg. Chim. Acta* **2000**, *298*, 97–102.
(55) Krejčík, M.; Daněk, M.; Hartl, F. *J. Electroanal. Chem.* **1991**, *317*, 179–187.
(56) Berger, R. M.; Mcmillin, D. R. *Inorg. Chem.* **1988**, *27*, 4245–4249.

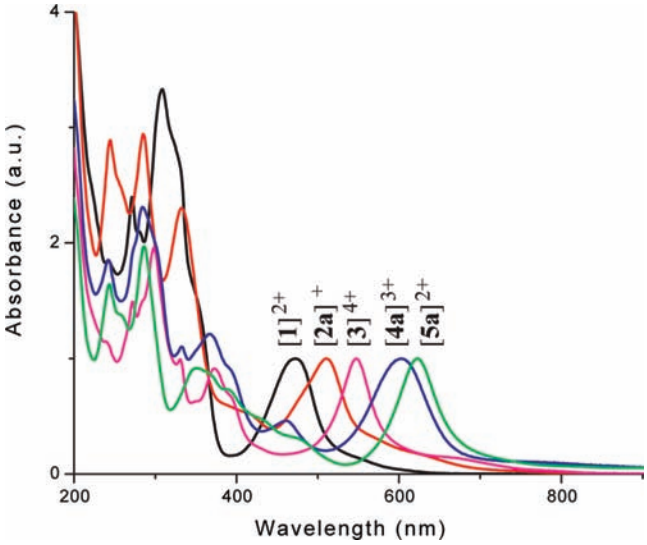

Figure 3. Electronic absorption spectra of $[\mathbf{1}]^{2+}$, $[\mathbf{2a}]^{+}$, $[\mathbf{3}]^{4+}$, $[\mathbf{4a}]^{3+}$, and $[\mathbf{5a}]^{2+}$ in MeCN.

Electronic Absorption Spectroscopy. The electronic absorption spectra of $[\mathbf{1}]^{2+}$, $[\mathbf{2a}]^{+}$, $[\mathbf{3}]^{4+}$, $[\mathbf{4a}]^{3+}$, and $[\mathbf{5a}]^{2+}$ (R = H) are depicted in Figure 3, and the spectral data for the entire series are listed in Table 3. All complexes exhibit strong absorptions in the UV region, assigned as intraligand $\pi-\pi^*$ transitions.[19,48−50] The visible absorption features are generally assigned to metal-to-ligand charge transfer (MLCT) transitions, in line with the ruthenium-based oxidation and ligand-based reductions. For the monoruthenium complexes, the transitions originate from the single ruthenium center, and the resulting excited state resides on the easily reducible tppz ligand. Destabilization of the ruthenium based levels because of the cyclometalation in $[\mathbf{2a}]^{+}$ results in a bathochromic shift of the MLCT band compared to $[\mathbf{1}]^{2+}$. Coordination of a second ruthenium-tpy center to the bridging tppz results in a strong bathochromic shift for $[\mathbf{3}]^{4+}$ compared to $[\mathbf{1}]^{2+}$, and for $[\mathbf{5a}]^{2+}$ compared to $[\mathbf{2a}]^{+}$, mainly as a result of the stabilized tppz acceptor states. Introduction of the second ruthenium moiety results in an approximately doubling of the molar absorption coefficient of the MLCT feature. Similar to the mononuclear complexes, cyclometalation causes red shifts of the main visible transition in $[\mathbf{5a}]^{2+}$ compared to $[\mathbf{3}]^{4+}$, with low-energy features extending down to 1100 nm. The visible absorption of the redox-asymmetric complex $[\mathbf{4a}]^{3+}$ is also shifted toward the low-energy region compared to $[\mathbf{3}]^{4+}$, but to a lesser extent than $[\mathbf{5a}]^{2+}$. The presence of the ester moiety in $[\mathbf{2b}]^{+}$, $[\mathbf{4b}]^{3+}$, and $[\mathbf{5b}]^{2+}$ results in a small blue shift of the visible absorption band compared to the corresponding unsubstituted complexes.

To obtain more insight into the electronic properties of this series, we investigated the nature of the lowest energy transitions using the time-dependent density functional theory (TD-DFT) approach. DFT is known to overestimate delocalization and therefore these results will be used in a qualitative sense only. Calculations were performed using the B3LYP functional with the DZ Dunning basis set[57,58] for all atoms except for ruthenium. For ruthenium the Stuttgart RSC 1997 ECP with relativistic core potential[59] was used. The complete applied basis set is given in the Supporting Information. TD-DFT calculations were run on optimized geometries at the same level of theory. The experimental spectra, electronic transitions predicted by TD-DFT, and the orbital energy diagrams of $[\mathbf{3}]^{4+}$, $[\mathbf{4a}]^{3+}$, and $[\mathbf{5a}]^{2+}$ are presented in Figure 4 and Table 4. A complete listing of electronic transitions, energy levels, and isovalue plots[60] of the frontier molecular orbitals for $[\mathbf{3}]^{4+}$, $[\mathbf{4a}]^{3+}$, $[\mathbf{4b}]^{3+}$, $[\mathbf{5a}]^{2+}$, $[\mathbf{5b}]^{2+}$ and one-electron oxidized $[\mathbf{3}]^{5+}$, $[\mathbf{4a}]^{4+}$, $[\mathbf{4b}]^{4+}$, $[\mathbf{5a}]^{3+}$, $[\mathbf{5b}]^{3+}$ can be found in the Supporting Information. In addition to the isovalue plots an extended Mulliken population analysis[61] was used to assign the nature of the individual orbitals, which can also be found in the Supporting Information. The studied complexes adopt similar geometries with the terminal ligands approximately perpendicular to the bridging ligand. The bridging ligand itself adopts a twisted conformation, with dihedral angles over the central pyrazine ring ranging from −13.7° to −17.7°, relieving steric hindrance between the pyridyl rings.

In the symmetric complexes $[\mathbf{3}]^{4+}$ and $[\mathbf{5a}]^{2+}$, the six highest occupied molecular orbitals (HOMOs) correspond to linear combinations of the ruthenium d_{xy}, d_{zx}, and d_{yz} orbitals with almost identical populations on the ruthenium atom (see Figure 5). We define the z-axis here as the longitudinal axis in the molecule and the x and y axes through the peripheral nitrogen atoms of the tppz and tpy ligands, respectively, Figure 5. In $[\mathbf{3}]^{4+}$, the HOMO is a linear combination of the d_{xy} orbitals from each ruthenium, while in $[\mathbf{5a}]^{2+}$ the HOMO is a linear combination of the d_{zx} and d_{yz} orbitals from each ruthenium. The Mulliken population on the ruthenium atoms for the HOMOs in cyclometalated $[\mathbf{5a}]^{2+}$ is somewhat decreased compared to the non-metalated $[\mathbf{3}]^{4+}$. Additionally, a component localized on the cyclometalated ligand is present in these levels. For the redox-asymmetric complexes $[\mathbf{4a}]^{3+}$ and $[\mathbf{4b}]^{3+}$ the situation is more complex, Figure 6. The three HOMOs can be assigned as localized on the cyclometalated ruthenium, with a component on the N,C,N'-bonded ligand. An orbital associated with the cyclometalated ligand is observed as HOMO−3 in $[\mathbf{4a}]^{3+}$, and as HOMO−4 in $[\mathbf{4b}]^{3+}$. At further decreased energies orbitals associated with the tpy-coordinated ruthenium are found.

The calculated electronic transitions correlate reasonably well with the experimental absorption spectra. One major electronic transition is predicted in the visible region, as well as a low-energy tail composed of multiple low-energy transitions. Even though the predicted transitions are consistently slightly blue-shifted, the trend in energy $[\mathbf{3}]^{4+} > [\mathbf{4b}]^{3+} \approx [\mathbf{4a}]^{3+} > [\mathbf{5b}]^{2+} \approx [\mathbf{5a}]^{2+}$ is completely obeyed. In both $[\mathbf{3}]^{4+}$, $[\mathbf{5a}]^{2+}$, and $[\mathbf{5b}]^{2+}$ the strong visible absorption originates from a MLCT transition originating from both metal centers and involving accepting states of the tppz bridge. In contrast to the large redox-asymmetry, the transitions in $[\mathbf{4a}]^{3+}$ and $[\mathbf{4b}]^{3+}$ are

(57) Dunning, T. H., Jr. *J. Chem. Phys.* **1970**, *53*, 2823–33.
(58) Dunning, T. H., Jr.; Hay, P. J. *Modern Theoretical Chemistry* **1977**, *3*, 1–27.
(59) Andrae, D.; Haussermann, U.; Dolg, M.; Stoll, H.; Preuss, H. *Theor. Chim. Acta.* **1990**, *77*, 123–141.
(60) Schaftenaar, G.; Noordik, J. H. *J. Comput. Aided Mater. Des.* **2000**, *14*, 123–134.
(61) Mulliken, R. S. *J. Chem. Phys.* **1955**, *23*, 1833–1840.

Table 3. Electronic Absorption Spectra of Complexes $[\mathbf{1}]^{2+}$–$[\mathbf{5}]^{2+}$ and Reference Compounds in MeCN

complex	λ_{max} (nm) (ε (10^3 M^{-1} cm^{-1})[a])
$[\mathbf{1}]^{2+}$	472 (17.1), 353 (sh), 309 (56.9), 271 (40.9)
$[\mathbf{2a}]^{+}$	511 (18.0), 403 (sh), 333 (41.4), 285 (53.0), 245 (52.0)
$[\mathbf{2b}]^{+}$	506 (18.2), 400 (sh), 333 (47.8), 284 (64.5), 243 (43.0)
$[\mathbf{3}]^{4+}$	667 (sh), 547 (37.3), 373 (34.1), 331 (37.1), 298 (72.9), 272 (55.2)
$[\mathbf{4a}]^{3+}$	768 (sh), 603 (33.0), 461 (15.2), 367 (40.0), 333 (36.4), 285 (76.1), 242 (61.1)
$[\mathbf{4b}]^{3+}$	760 (sh), 597 (39.2), 460 (14.5), 369 (42.5), 332 (43.5), 283 (93.3), 241 (56.6)
$[\mathbf{5a}]^{2+}$	1050 (1.9), 900 (2.5), 622 (45.2), 470 (sh), 392 (sh), 351 (41.5), 286 (88.9), 244 (74.3)
$[\mathbf{5b}]^{2+}$	990 (1.5), 866 (sh), 614 (44.1), 467 (sh), 382 (sh), 345 (45.9), 284 (109.4), 242 (63.5)
$[(RuCl(L))_2(\mu\text{-tppz})]$ [b]	625 (19.0), 347 (50.4), 248 (46.1)
$[(RuCl(bpy))_2(\mu\text{-tppz})]^{2+}$ [c]	598 (30.3), 436 (15.4)

[a] sh = shoulder. [b] Ref 24. [c] Ref 25.

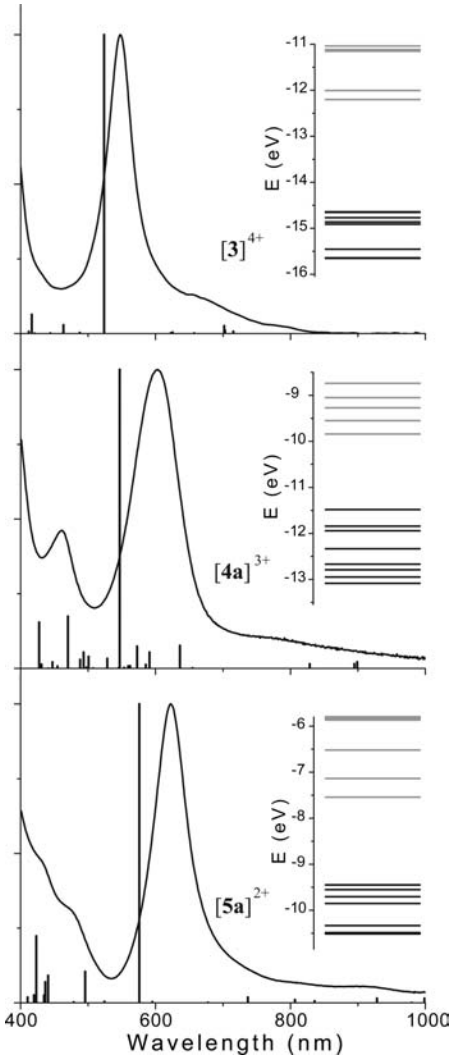

Figure 4. UV–vis spectra of (a) $[\mathbf{3}]^{4+}$ (top), (b) $[\mathbf{4a}]^{3+}$ (middle), and (c) $[\mathbf{5a}]^{2+}$ (bottom) in MeCN (line). Excitations predicted by TD-DFT in vacuo are shown as black bars. Inset: orbital energy diagrams (occupied and unoccupied MOs represented by black and gray lines, respectively).

also assigned an MLCT character, with contribution from both the cyclometalated and non-metalated ruthenium centers. Transitions having almost pure cyclometalated-ruthenium-to-tppz MLCT character correspond to the structured low-intensity red tails.

Spectroelectrochemistry. One-electron oxidation of complex $[\mathbf{3}]^{4+}$ in MeCN results in partial disappearance of the visible MLCT absorption. A new strong band in the NIR region has been assigned to the intervalence charge transfer transition.[21,25,26,62,63] One-electron oxidation of complexes $[\mathbf{5a}]^{2+}$ and $[\mathbf{5b}]^{2+}$ with $[Ce(NO_3)_6](NH_4)_2$ in CD_3CN also diminished the visible MLCT absorptions and gave rise to a strong, narrow band in the NIR, Figure 7 and Table 5. The parent complexes could be fully regenerated by addition of ferrocene. The NIR band of $[\mathbf{5a}]^{3+}$ is centered at 1661 nm, with $\Delta\nu_{1/2} = 1033$ cm^{-1} being significantly narrower than predicted by the value of 3720 cm^{-1} calculated from the Hush formula ($\Delta\nu_{1/2} = (16RT \ln 2(\nu_{max}))^{1/2}$, $R = 0.695$ cm^{-1} K^{-1}, $T = 298$ K, $\nu_{max} = 6020$ cm^{-1}),[64] applicable for weakly coupled, localized, class II mixed-valence systems. The NIR absorption bands in $[\mathbf{5a}]^{3+}$ and $[\mathbf{5b}]^{3+}$ are, like the main NIR absorption of $[\mathbf{3}]^{5+}$, largely solvent independent, see Table 5.

We have also used DFT calculations as an indicative analytical tool for the one-electron oxidized mixed valence complexes. However, the tendency of DFT to overestimate delocalization makes this method less suitable for these large and delocalized systems. The overall features of the spectra are well predicted, but the experimental trends in energy were not reproduced. The results of these calculations are summarized in the Supporting Information but are very scarcely covered within this paper.

Table 4. Major Low-Energy Electronic Transitions Calculated by TD-DFT for $[\mathbf{3}]^{4+}$, $[\mathbf{4}]^{3+}$, and $[\mathbf{5}]^{2+}$, Wavelength (nm), Oscillator Strength (f), and Assignment

	λ_{max} (exp) (nm)[a]	No.[b]	λ_{max} (dft) (nm)	f	Composition (c^2)[c]
$[\mathbf{3}]^{4+}$	547	10	524	0.5685	H-1 → L+1 (0.28)
					H → L (0.054)
$[\mathbf{4a}]^{3+}$	603	15	547	0.3763	H-4 → L (0.22)
					H-3 → L (0.03)
					H-2 → L+1 (0.12)
$[\mathbf{4b}]^{3+}$	597	16	549	0.3898	H-6 → L (0.10)
					H-5 → L (0.08)
					H-2 → L+1 (0.12)
$[\mathbf{5a}]^{2+}$	622	11	576	0.4687	H-3 → L (0.07)
					H-2 → L+1 (0.20)
					H → L+1 (0.06)
$[\mathbf{5b}]^{2+}$	614	11	573	0.5559	H-3 → L (0.07)
					H-2 → L+1 (0.17)
					H → L+ 1 (0.10)

[a] See Figure 4. [b] Numbers of the predicted transitions; a complete listing can be found in the Supporting Information. [c] Weight of the orbital transition component in the electronic excitation.

(62) Gourdon, A.; Launay, J. P. *Inorg. Chem.* **1998**, *37*, 5336–5341.
(63) Ruminski, R.; Kiplinger, J.; Cockroft, T.; Chase, C. *Inorg. Chem.* **1989**, *28*, 370–373.
(64) D'Alessandro, D. M.; Keene, F. R. *Chem. Soc. Rev.* **2006**, *35*, 424–440.

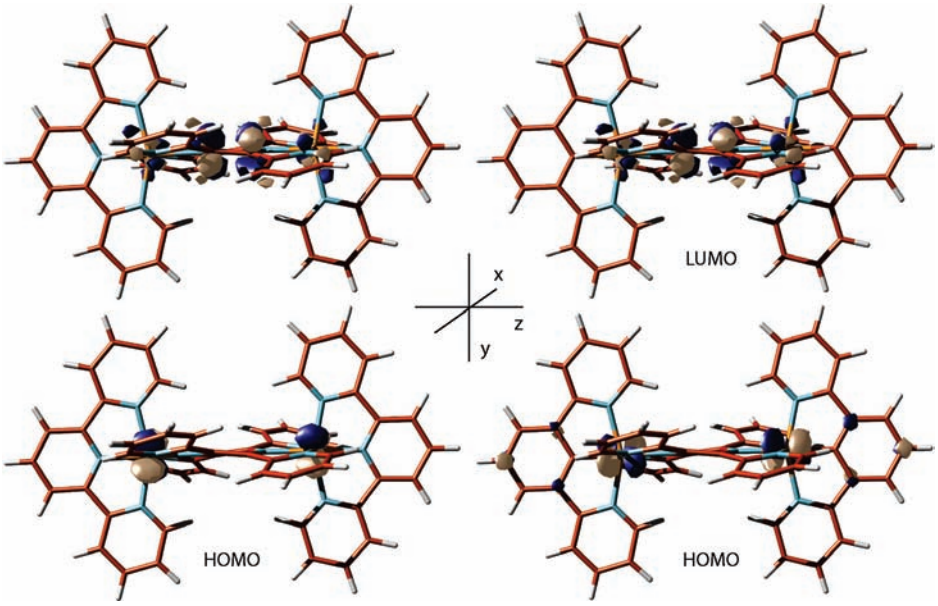

Figure 5. Isovalue (value = 0.05) plots of the HOMO (bottom) and LUMO (top) of $[\mathbf{3}]^{4+}$ (left) and $[\mathbf{5a}]^{2+}$ (right).

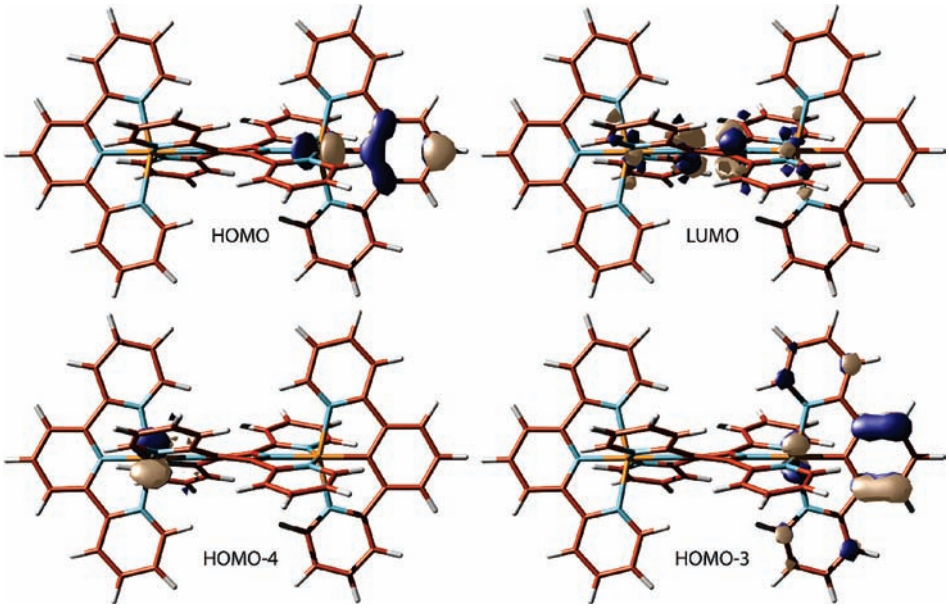

Figure 6. Isovalue (value = 0.05) plots of selected molecular orbitals of $[\mathbf{4a}]^{3+}$.

One-electron oxidation of complex $[\mathbf{4b}]^{3+}$ using $[Ce(NO_3)_6](NH_4)_2$ in MeCN also diminished the visible MLCT band, albeit to a lesser extent than in the case of $[\mathbf{3}]^{5+}$, $[\mathbf{5a}]^{3+}$, and $[\mathbf{5b}]^{3+}$; it also shifted hypsochromically its absorption maximum from 614 to 523 nm, Figure 8, with a distinct shoulder visible at 650 nm. In addition to these changes, a weak NIR feature appeared centered at 1050 nm. Back reduction with ferrocene completely restored the UV−vis spectrum of parent $[\mathbf{4b}]^{3+}$. A similar picture is obtained for $[\mathbf{4a}]^{4+}$ in which the low-energy transition is hypsochromically shifted and obscured by the LMCT shoulder.

Emission Spectroscopy. Room temperature phosphorescence from monometallic, non-metalated $[\mathbf{1}]^{2+}$ has been reported at 670 nm.[28,36] The dimetallic complex $[\mathbf{3}]^{4+}$ emits at 820 nm. Since all studied cyclometalated complexes have a weak absorption tailing far into the NIR, no emission of complexes $[\mathbf{2}]^{2+}$, $[\mathbf{4a}]^{3+}$, $[\mathbf{4b}]^{3+}$, $[\mathbf{5a}]^{2+}$, and $[\mathbf{5b}]^{2+}$ was detected below 900 nm.

Discussion

Redox-Symmetric Complexes. Strong σ-donation from the formally anionic carbon in $[\mathbf{5a}]^{2+}$ negatively shifts the initial metal-based oxidation potential. This is reflected by an increase in the electron density on the ruthenium ions as revealed by an increase in total Mulliken population from 15.08 electron per metal center in $[\mathbf{3}]^{4+}$ to 15.27 electron in $[\mathbf{5a}]^{2+}$. Additionally, a component on the cyclometalated ligand is present in the HOMOs, while the ruthenium character is slightly suppressed. However, the HOMOs are still well described as metal-based. These electron-rich ruthenium centers cause an increased back-donation to the bridging tppz ligand, as evidenced by the changing chemical shift of its protons and the negative

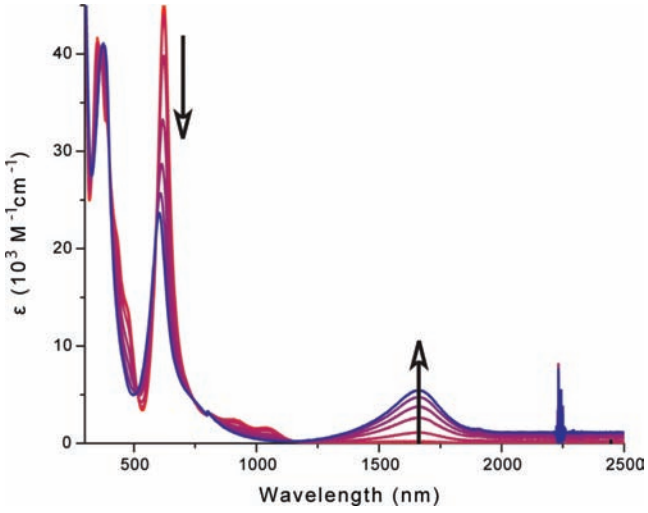

Figure 7. UV−vis−NIR spectra recorded during chemical oxidation of $[\mathbf{5a}]^{2+}$ to $[\mathbf{5a}]^{3+}$ Ce(IV) in CD_3CN.

Table 5. IVCT Transitions for One-Electron Oxidized $[\mathbf{3}]^{5+}$, $[\mathbf{5a}]^{3+}$, and $[\mathbf{5b}]^{3+}$

	$[\mathbf{3}]^{5+}$	$[\mathbf{5a}]^{3+}$	$[\mathbf{5b}]^{3+}$
K_c	2.6×10^5	5.4×10^4	3.8×10^5
	λ_{max}(exp) (nm) (ε (10^3 M^{-1} cm^{-1}) ($\Delta\tilde{\nu}_{1/2}$ (cm^{-1})))		
CD_3CN[a]	1527 (7.6) (970)[c]	1661 (5.5) (1033)	1686 (7.5) (1062)
acetone-d6[a]		1669 (4.0) (1176)	1702 (6.0) (1129)
CD_2Cl_2[b]	1519 (nd) (1119)[d]	1653 (6.2) (932)	1672 (7.5) (935)

[c]Oscillator strength. [a]Chemical oxidation performed using a $[Ce(NO_3)_6](NH_4)_2$ solution in the appropriate solvent. [b]Chemical oxidation performed using a $SbCl_5$ solution in CD_2Cl_2. [c]Ref 21. [d]Experiment performed in nondeuterated solvent.

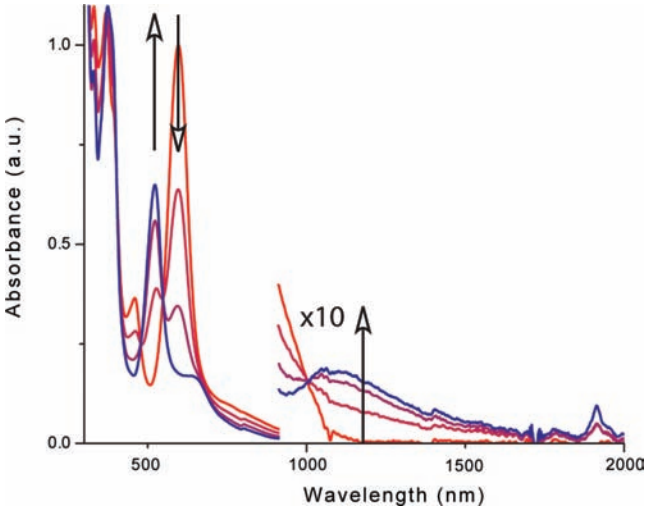

Figure 8. UV−vis spectra recorded during the chemical oxidation of $[\mathbf{4b}]^{3+}$ to $[\mathbf{4b}]^{4+}$ with Ce(IV) in MeCN.

shift of the initial reduction potential. The main visible absorption feature in $[\mathbf{3}]^{4+}$, $[\mathbf{5a}]^{2+}$, and $[\mathbf{5b}]^{2+}$ is well predicted by TD-DFT calculations and corresponds to a single MLCT transition with equal contribution from each ruthenium center to the donating state and the tppz ligand acting as accepting state. The large negative shift of the oxidation potential corresponds with the observed red shifts of the absorption feature.

Substitution with the ester moiety dampens the effect of the anionic carbon in all cyclometalated complexes. The negative shifts of the potential of the initial oxidation and reduction processes are less pronounced. As a consequence the corresponding red shift of the visible absorption features is smaller in $[\mathbf{5b}]^{2+}$ as compared to $[\mathbf{5a}]^{2+}$. The upfield shift of the ^1H NMR resonances for the protons on the peripheral ligand compared to the resonances for the non-metalated $[\mathbf{3}]^{4+}$ is decreased, as is the trend in the chemical shift for the bridging tppz ligand. Furthermore, the resonance assigned to the C_{ipso} A1 in $[\mathbf{5a}]^{2+}$ is upfield shifted compared to that in the ester disubstituted complex $[\mathbf{5b}]^{2+}$, reflecting a more electron rich metalated carbon atom in $[\mathbf{5a}]^{2+}$.

In general, $\Delta E_{1/2}$(ox) is used as a measure of the extent of electronic communication between metal centers in a redox-symmetric dinuclear assembly. One has to keep in mind, however, that other effects can also play a non-negligible role, such as the nature of the anion of the electrolyte.[65−67] The separation of the oxidation waves ($\Delta E_{1/2}$(ox) = 0.32 V) in $[\mathbf{3}]^{4+}$ is an indication for a strong electronic communication between the two ruthenium centers across the tppz bridging ligand.[21,28] For $[\mathbf{5a}]^{2+}$ (0.28 V) this value is slightly decreased, while it is slightly increased for $[\mathbf{5b}]^{2+}$ (0.33 V). In each case, Mulliken population analysis did not show any localization of the metal-based levels. However, because of the artificial preference of DFT methods for delocalization,[68−70] extreme care has to be taken in the analysis of the resulting data since delocalization, and hence the estimated metal−metal interaction, might be overestimated. It is interesting to note that a decrease in the electron density at the ruthenium centers in tppz bridged dimers, resulting from strongly π-acidic terminal ligands, has been found to result in decreased electronic coupling between the ruthenium centers,[22,24] that is, the reduced π-back-bonding to the tppz is responsible for a lower degree of electronic communication through the unoccupied levels. However, the strongly σ-donating, weakly π-accepting, anionic cyclometalated ligands in $[\mathbf{5a}]^{2+}$ (R = H) and $[\mathbf{5b}]^{2+}$ (R = CO_2Me) result in strong π-back-bonding to the tppz ligands but do not significantly increase the comproportionation constants for $[\mathbf{5a}]^{3+}$ and $[\mathbf{5b}]^{3+}$ compared to $[\mathbf{3}]^{5+}$. The increased electronic communication through the unoccupied levels is likely offset by decreased communication through the occupied levels. As the metal levels are destabilized, the energetic matching with the occupied tppz levels is decreased, and a maximum interaction is reached.

The narrow IVCT band of $[\mathbf{3}]^{5+}$ is indicative of the Robin-Day class III behavior.[71] It has to be noted that the terms "IVCT" and "mixed valence" are retained for class III compounds, although the NIR transitions do not involve net charge transfer and the systems are more accurately defined as "average valence" $[Ru^{IIS}Ru^{IIS}]$.[64] However, some features of $[\mathbf{3}]^{5+}$ cannot be reconciled

(65) Flanagan, J. B.; Margel, S.; Bard, A. J.; Anson, F. C. *J. Am. Chem. Soc.* **1978**, *100*, 4248–4253.
(66) Glockle, M.; Katz, N. E.; Ketterle, M.; Kaim, W. *Inorg. Chim. Acta* **2002**, *336*, 55–60.
(67) D'Alessandro, D. M.; Keene, F. R. *Dalton Trans.* **2004**, 3950–3954.
(68) Gruning, M.; Gritsenko, O. V.; van Gisbergen, S. J. A.; Baerends, E. J. *J. Phys. Chem. A* **2001**, *105*, 9211–9218.
(69) Sodupe, M.; Bertran, J.; Rodriguez-Santiago, L.; Baerends, E. J. *J. Phys. Chem. A* **1999**, *103*, 166–170.
(70) Dreuw, A.; Head-Gordon, M. *J. Am. Chem. Soc.* **2004**, *126*, 4007–4016.
(71) Robin, M. B.; Day, P. *Adv. Inorg. Chem. Radiochem.* **1967**, *10*, 247–422.

with pure class III behavior,[3,21] in particular the solvatochromic, low intensity band at 2850 nm. As for $[\mathbf{3}]^{5+}$ the NIR band for $[\mathbf{5a}]^{3+}$ or $[\mathbf{5b}]^{3+}$ is narrow and indicative for class III behavior. This is in line with the absence of solvatochromism of the NIR bands, Table 5. The assignment of the NIR band in $[\mathbf{5a}]^{3+}$ and $[\mathbf{5b}]^{3+}$ from TD-DFT seems to contain some additional LMCT component originating from the tppz ligand. Again, the strong σ-donating and weak π-accepting anionic cyclometalated ligands in $[\mathbf{5a}]^{3+}$ and $[\mathbf{5b}]^{3+}$ do not seem to result in significantly altered interaction.

Redox-Unsymmetrical Complexes. The singly cyclometalated complexes $[\mathbf{4a}]^{3+}$ and $[\mathbf{4b}]^{3+}$ feature an apparent redox-asymmetry, the initial oxidation being assigned to the cyclometalated ruthenium center. However, the second anodic step is not associated with the non-metalated ruthenium but rather with the cyclometalated ligand. This process is electrochemically irreversible, unlike what is expected for a ruthenium-based oxidation. Furthermore, an orbital localized on the cyclometalated ligand is predicted by DFT at a higher energy compared to levels associated with the non-metalated ruthenium center, in both the parent and the one-electron-oxidized species. The initial reduction potential of the tppz ligand is shifted negatively by back-donation from the electron-rich ruthenium center shifts, albeit to a lesser extent than for $[\mathbf{5a}]^{2+}$ and $[\mathbf{5b}]^{2+}$, as only one cyclometalated ruthenium center is present. The presence of a single visible absorption feature for $[\mathbf{4a}]^{3+}$ and $[\mathbf{4b}]^{3+}$ indicates strong electronic communications, as transitions associated with the individual centers would be observed otherwise. Indeed, irrespective of the large redox-asymmetry between the metal centers, the transition can be assigned to a MLCT excitation involving both ruthenium atoms.

One-electron oxidation of $[\mathbf{4a}]^{3+}$ and $[\mathbf{4b}]^{3+}$ result in similar changes in the UV−vis−NIR spectra. However, the individual bands are more clearly observed in $[\mathbf{4b}]^{4+}$ as they overlap in $[\mathbf{4a}]^{4+}$. The visible MLCT band of $[\mathbf{4b}]^{3+}$ is diminished upon oxidation, albeit to a lesser extent than is observed for $[\mathbf{3}]^{5+}$, $[\mathbf{5a}]^{3+}$, and $[\mathbf{5b}]^{3+}$. More importantly, the significant difference in λ_{max} reflects a change in the character from the original MLCT to a persisting MLCT (M = RuN_6) transition. In addition to these changes, a weak NIR feature appears centered at 1050 nm. The combination of two strongly interacting unequal metal centers with a ligand-based second oxidation results in a low-energy band that does not display features expected for an asymmetric IVCT type transition but rather of an LMCT transition.

Conclusions

To investigate the consequences of cyclometalation on electronic communication between metal centers in a dinuclear assembly, we have used the well-known tppz ligand to prepare a series of bridged bisorganoruthenium complexes, with cyclometalated peripheral ligands. Because of the covalent, σ Ru−C bond between a formal anionic carbon and the ruthenium ion instead of a coordinative nitrogen-to-ruthenium bond, the electronic properties are dramatically changed, without significantly affecting the geometry of the resulting complex. Strong σ-donation results in electron rich metal centers that respond by increased back-donation to the tppz bridging ligand.

The electronic spectra of the cyclometalated complexes display large bathochromic shifts of the dominant MLCT transition in the visible region, as well as the low-energy absorption tailing into the NIR region. Introduction of an electron withdrawing ester substituent at the cyclometalated ligand partly decreases the donor character of the anionic carbon center, and consequently tempers the effects of cyclometalation. Although back-donation to the bridging ligand is significantly increased, the comproportionation constants of cyclometalated $[\mathbf{5a}]^{3+}$ and $[\mathbf{5b}]^{3+}$ are similar to the value obtained for non-cyclometalated $[\mathbf{3}]^{5+}$. Oxidation into the mixed valence state resulted in the appearance of NIR electronic transitions, with high values of molar absorption coefficients and small bandwidths, characteristic for Robin-Day class III compounds.

The redox asymmetric complexes $[\mathbf{4a}]^{3+}$ and $[\mathbf{4b}]^{3+}$, containing only one σ carbon-to-ruthenium bond, show a single visible MLCT absorption of energy intermediate between $[\mathbf{3}]^{4+}$, $[\mathbf{5a}]^{2+}$, and $[\mathbf{5b}]^{2+}$. Being associated with both ruthenium centers, this electronic excitation is indicative of delocalization throughout the molecule. The anodic potential of the reversible first, ruthenium based oxidation is strongly negatively shifted compared to $[\mathbf{3}]^{4+}$. However, the second oxidation potential is chemically irreversible and associated with the cyclometalated ligand. One-electron oxidation gives rise to a weak low-energy absorption band.

Experimental Section

General Procedures. All air-sensitive reactions were performed under a dry nitrogen atmosphere using standard Schlenk techniques. Solvents were dried over appropriate drying agents and distilled before use. All other solvents and reagents were purchased and used as received. ^{1}H and ^{13}C{1H} NMR spectra were recorded at 298 K on a Varian 300 MHz Inova spectrometer and on a Varian 400 MHz NMR system. NMR spectra were referenced to the solvent residual signal.[72] Spectral assignments were based on chemical shift and integral considerations as well as COSY and NOESY two-dimensional experiments. Elemental analyses were carried out by Kolbe Mikroanalytisches Laboratorium (Mülheim an der Ruhr, Germany). Neutral Al_2O_3 was obtained from Across and deactivated to Brockmann grade 3. Compounds tppz,[18] $[\mathbf{1}]^{2+}$,[36] $[\mathbf{3}]^{4+}$,[27,28] $[RuCl_2(\eta^6\text{-}C_6H_6)]_2$,[73] N^C(H)^N,[40] MeO_2C−N^C(H)^N,[41,51] and $[(RuCl_3)_2(\mu\text{-tppz})]$[25] were prepared by literature procedures.

Electronic Spectroscopic Measurements and Electrochemical Experiments. Electronic absorption spectra were recorded on a Cary 50 Scan UV−vis spectrophotometer, or on a Cary 5 UV−vis−NIR spectrophotometer. Chemical oxidation of samples was performed by titration with 4 mM $[Ce(NO_3)_6](NH_4)_2$ in MeCN. Cyclic voltammograms were recorded in a single-compartment cell under a dry nitrogen atmosphere. The cell was equipped with a Pt microdisk working electrode, Pt wire auxiliary electrode, and a Ag/AgCl wire reference electrode. The working electrode was polished with Alumina nano powder between scans. The potential control was achieved with a PAR Model 263A potentiostat. All redox potentials are reported against the ferrocene-ferrocenium (Fc/Fc^+) redox couple used as an internal standard.[53,54] All electrochemical samples were 10^{-1} M in $[n\text{-}Bu_4N]PF_6$ as the supporting electrolyte in CH_3CN distilled over $KMnO_4$ and Na_2CO_3.

UV−vis Spectroelectrochemical Measurements. All the experiments were performed with an optically transparent thin-layer

(72) Gottlieb, H. E.; Kotlyar, V.; Nudelman, A. *J. Org. Chem.* **1997**, *62*, 7512–7515.
(73) Zelonka, R. A.; Baird, M. C. *Can. J. Chem.* **1972**, *50*, 3063–3072.

electrochemical (OTTLE) cell,[55] equipped with a Pt minigrid working electrode and quartz optical windows. The controlled potential electrolyses were carried out with a PA4 potentiostat (EKOM, Polná, Czech Republic). All electrochemical samples were 10^{-1} M in $[n\text{-}Bu_4N]PF_6$ in freshly distilled CH_3CN and THF. UV−vis spectra were recorded with a Hewlett-Packard 8453 diode-array spectrophotometer.

DFT calculations. DFT calculations were performed using the B3LYP functional and the DZ Dunning[57,58] basis set for all atoms except ruthenium. The Stuttgart RSC 1997 ECP with relativistic core potential[59] was applied for ruthenium. Geometries were optimized using the GAMESS-UK[74] program package. Subsequent TD-DFT calculations were run on the optimized geometry at the same level of theory using the Gaussian[75] 03 program package. Isovalue plots of the frontier molecular orbitals were made using MOLDEN.[60]

Syntheses. [Ru(N^C^N)(MeCN)$_3$](PF$_6$), [6a](PF$_6$). The ligand N^C(H)^N (222 mg, 0.96 mmol) was added to a suspension of $[RuCl_2(\eta^6\text{-}C_6H_6)]_2$ (239 mg, 0.48 mmol), KPF_6 (376, 2.0 mmol), and crushed NaOH (50 mg, 1.25 mmol) in dry MeCN (30 mL). The resulting mixture was stirred at 45 °C for 15 h. The orange solution was filtered under inert atmosphere over 15 cm of Al_2O_3 (MeCN) and concentrated in vacuo, yielding the product as a dark orange solid (0.47 g, 82%). ^{1}H NMR showed the presence of a mixture of compounds, but the product could be used in subsequent reactions without further purification.

[Ru(MeO$_2$C−N^C^N)(MeCN)$_3$](PF$_6$), [6b](PF$_6$). A mixture of MeO$_2$C−N^C(H)^N (62 mg, 0.2 mmol), $[RuCl_2(\eta^6\text{-}C_6H_6)]_2$ (52 mg, 0.1 mmol), crushed NaOH (8 mg, 0.2 mmol), and KPF_6 (80 mg, 0.4 mmol) in dry MeCN (4 mL) was stirred at 40 °C for 15 h. The orange solution was filtered under inert atmosphere over 15 cm of Al_2O_3 (MeCN) and concentrated to 0.5 mL. Crystallization was induced by careful addition of dry Et_2O (10 mL), and the crystals were washed with Et_2O (10 mL), yielding the product as a orange solid (91 mg, 69%). Single crystals suitable for X-ray analysis were obtained by slow diffusion of Et_2O into a MeCN solution.

^{1}H NMR (400 MHz, CD_3CN): δ 8.89 (d, 2H, ^3J = 5.6 Hz, B6), 8.47 (s, 2H, A3,5), 8.16 (d, 2H, ^3J = 8.0 Hz, B3), 7.91 (dd, 2H, ^3J = 8.0 Hz, ^3J = 7.6 Hz, B4), 7.33 (dd, 2H, ^3J = 7.6 Hz, ^3J = 5.6 Hz, B5), 3.94 (s, 2H, CO_2CH_3), 2.14 (s, 3H, MeCN), 1.77 (s, 6H, MeCN).

^{13}C NMR (100 MHz, CD_3CN): δ 226.2, 168.9, 168.3, 154.7, 146.6, 137.5, 123.7, 123.6, 122.7, 120.3, 52.4, 3.7, not all MeCN signals could be resolved.

[(N^C^N)Ru(tppz)](PF$_6$), [2a]$^+$. A suspension of tppz (550 mg, 1.46 mmol) in DMF (12 mL) was added to [**6a**](PF$_6$) (220 mg, 0.367 mmol). The resulting solution was heated under reflux for 3 h. An excess of KPF_6 was added, and the solution poured into H_2O (80 mL), which resulted in the precipitation of the complex. The product was isolated by filtration, collected with a minimum of MeCN, and was purified by column chromatography on SiO_2 (MeCN/aq. 0.5 M $NaNO_3$ = 9:1) and on Al_2O_3 (Et_2O/MeCN = 2: 1). After anion exchange, the product was obtained as a dark red solid (11 mg, 11%).

^{1}H NMR (400 MHz, CD_3CN): δ 8.74 (d, 2H, ^3J = 5.6 Hz, B3), 8.30 (d, 2H, ^3J = 7.6 Hz, A3,5), 8.29 (d, 2H, ^3J = 8.0 Hz, D6), 8.16−8.22 (m, 4H, D3 + D5), 7.62−7.70 (m, 4H, D4 + B4), 7.53 (t, 1H, ^3J = 7.6 Hz, A4), 7.42 (d, 2H, ^3J = 7.6 Hz, C3), 7.37 (dd, 2H, ^3J = 7.6 Hz, ^3J = 7.6 Hz, C4), 7.25 (d, 2H, ^3J = 5.6 Hz, C6), 7.15 (d, 2H, ^3J = 5.6 Hz, B6), 6.93 (dd, 2H, ^3J = 7.6 Hz, ^3J = 5.6 Hz, C5), 6.71 (dd, 2H, ^3J = 7.6 Hz, ^3J = 5.6 Hz, B5).

^{13}C NMR (100 MHz, CD_3CN): δ 220.3, 169.5, 158.9, 156.8, 154.9, 152.9, 151.8, 150.8, 146.1, 152.0, 139.2, 137.2, 135.1, 127.8, 127.3, 126.5, 126.3, 125.2, 122.6, 122.3, 120.9.

Anal. Calcd for $C_{40}H_{27}F_6N_8PRu$: C, 55.49; H, 3.14; N, 12.94. Found: C, 55.47; H, 3.20; N, 12.99.

MALDI-TOF-MS (DHB Matrix): m/z = 721.17 [M$^+$] (calcd for $C_{40}H_{27}N_8Ru$, 721.14).

[(MeO$_2$C−N^C^N)Ru(tppz)](PF$_6$), [2b]$^+$. A suspension of tppz (100 mg, 0.25 mmol) in DMF (6 mL) was added to [**6b**](PF$_6$) (21 mg, 0.041 mmol). The resulting solution was heated under reflux for 3 h. An excess of KPF_6 was added, and the solution poured into H_2O (80 mL), which resulted in the precipitation of the complex. The product was isolated by filtration, collected with a minimum of MeCN, and was purified by column chromatography on SiO_2 (MeCN/aq. 0.5 M $NaNO_3$ = 9: 1). After anion exchange, the product was obtained as a dark red solid (31 mg, 95%).

^{1}H NMR (400 MHz, CD_3CN): δ 8.89 (s, 2H, A3,5), 8.73 (d, 2H, ^3J = 4.8 Hz, B3), 8.28−8.34 (m, 4H, D6 + D3), 8.19 (dd, 2H, ^3J = 7.6 Hz, ^3J = 7.6 Hz, D5), 7.66−7.72 (m, 4H, D4 + B4), 7.44 (d, 2H, ^3J = 8.0 Hz, C3), 7.37 (dd, 2H, ^3J = 8.0 Hz, ^3J = 7.6 Hz, C4), 7.25 (d, 2H, ^3J = 5.6 Hz, B6), 7.20 (d, 2H, ^3J = 5.6 Hz, C6), 6.89 (dd, 2H, ^3J = 7.6 Hz, ^3J = 5.6 Hz, C5), 6.78 (dd, 2H, ^3J = 7.6 Hz, ^3J = 5.6 Hz, B5), 4.06 (s, 3H, CO_2CH_3).

^{13}C NMR (100 MHz, CD_3CN): δ 230.3, 168.9, 168.6, 158.6, 156.6, 155.0, 152.9, 151.7, 150.8, 145.6, 142.4, 139.3, 137.4, 135.6, 128.0, 127.4, 126.6, 126.3, 125.1, 124.2, 123.3, 121.4, 52.7.

Anal. Calcd for $C_{42}H_{29}F_6N_8O_2PRu \cdot 2H_2O$: C, 52.56; H, 3.47; N, 11.67. Found: C, 52.60; H, 3.41; N, 11.15.

MALDI-TOF-MS (DHB Matrix): m/z = 779.14 [M$^+$] (calcd for $C_{42}H_{29}N_8O_2Ru$, 779.15).

[(tpy)Ru(μ-tppz)Ru(N^C^N)](PF$_6$)$_3$, [4a]$^{3+}$. A solution of [**1**](PF$_6$)$_2$ (105 mg, 0.1 mmol) and [**6a**](PF$_6$) (200 mg, 0.33 mmol) in DMF (20 mL) was heated under reflux for 3 h. The product was isolated by concentration in vacuo, dissolution in acetone, and precipitation by addition of an excess of KPF_6 in H_2O. The product was purified by column chromatography on SiO_2 (MeCN/aq. 0.5 M $NaNO_3$ = 9: 1), anion exchange, and crystallization by slow evaporation of a solution in acetone/toluene. The product was obtained as a dark turquoise solid (87 mg, 59%).

^{1}H NMR (400 MHz, CD_3CN): δ 8.95 (d, 2H, ^3J = 8.0 Hz, C3), 8.89 (d, 4H, ^3J = 8.0 Hz, F3,5 + D3), 8.63 (d, 2H, ^3J = 8.0 Hz, E3), 8.58 (t, 1H, ^3J = 8.0 Hz, F4), 8.41 (d, 2H, ^3J = 7.6 Hz, A3,5), 8.27 (d, 2H, ^3J = 8.0 Hz, B3), 8.06 (dd, 2H, ^3J = 8.0 Hz, ^3J = 7.6 Hz, E4), 7.88 (dd, 2H, ^3J = 8.0 Hz, ^3J = 8.0 Hz, D4), 7.82 (d, 2H, ^3J = 5.2 Hz, E6), 7.76 (m, 4H, B4 + C4), 7.68 (d, 2H, ^3J = 5.2 Hz, D6), 7.66 (t, 1H, ^3J = 7.6 Hz, A4), 7.65 (d, 2H, ^3J = 6.4 Hz, C6), 7.30−7.36 (m, 4H, E5 + D5), 7.24−7.30 (m, 4H, B6 + C5), 6.80 (dd, 2H, ^3J = 5.6 Hz, ^3J = 7.6 Hz, B5).

^{13}C NMR (100 MHz, CD_3CN): δ 217.6, 169.2, 158.8, 157.2, 157.1, 156.3, 156.0, 154.7, 154.2, 154.2, 148.7, 148.0, 141.9, 139.7, 138.6, 138.1, 138.0, 136.0, 129.7, 129.5, 129.4, 129.2, 128.8, 125.8, 125.7, 125.3, 123.7, 123.0, 121.2.

Anal. Calcd for $C_{55}H_{38}F_{18}N_{11}P_3Ru_2$: C, 44.33; H, 2.57; N, 10.34. Found: C, 44.45; H, 2.49; N, 10.26.

MALDI-TOF-MS (DHB Matrix): m/z = 1056.07 [M$^+$] (calcd for $C_{55}H_{38}N_{11}Ru_2$, 1056.14).

(74) Guest, M. F.; Bush, I. J.; van Dam, H. J. J.; Sherwood, P.; Thomas, J. M. H.; van Lenthe, J. H.; Havenith, R. W. A.; Kendrick, J. *Mol. Phys.* **2005**, *103*, 719–747.

(75) Frisch, M. J.; Trucks, G. W.; Schlegel, H. B.; Scuseria, G. E.; Robb, M. A.; Cheeseman, J. R.; Montgomery, J., J. A.; Vreven, T.; Kudin, K. N.; Burant, J. C.; Millam, J. M.; Iyengar, S. S.; Tomasi, J.; Barone, V.; Mennucci, B.; Cossi, M.; Scalmani, G.; Rega, N.; Petersson, G. A.; Nakatsuji, H.; Hada, M.; Ehara, M.; Toyota, K.; Fukuda, R.; Hasegawa, J.; Ishida, M.; Nakajima, T.; Honda, Y.; Kitao, O.; Nakai, H.; Klene, M.; Li, X.; Knox, J. E.; Hratchian, H. P.; Cross, J. B.; Bakken, V.; Adamo, C.; Jaramillo, J.; Gomperts, R.; Stratmann, R. E.; Yazyev, O.; Austin, A.; J.; Cammi, R.; Pomelli, C.; Ochterski, J. W.; Ayala, P. Y.; Morokuma, K.; Voth, G. A.; Salvador, P.; Dannenberg, J. J.; Zakrzewski, V. G.; Dapprich, S.; Daniels, A. D.; Strain, M. C.; Farkas, O.; Malick, D. K.; Rabuck, A. D.; Raghavachari, K.; Foresman, J. B.; Ortiz, J. V.; Cui, Q.; Baboul, A. G.; Clifford, S.; Cioslowski, J.; Stefanov, B. B.; Liu, G.; Liashenko, A.; Piskorz, P.; Komaromi, I.; Martin, R. L.; Fox, D. J.; Keith, T.; Al-Laham, M. A.; Peng, C. Y.; Nanayakkara, A.; Challacombe, M.; Gill, P. M. W.; Johnson, B.; Chen, W.; Wong, M. W.; Gonzalez, C.; Pople, J. A. *Gaussian 03*; Gaussian, Inc: Wallingford, CT, 2004.

[(MeO$_2$C−N^C^N)Ru(μ-tppz)Ru(tpy)](PF$_6$)$_3$, [4b]$^{3+}$. A solution of [**1**](PF$_6$)$_2$ (57 mg, 0.056 mmol) in DMF (6 mL) was added to [**6b**](PF$_6$) (34 mg, 0.052 mmol). The resulting solution was heated under reflux for 3 h. An excess of KPF_6 was added, and the solution poured into H_2O (80 mL), which resulted in the precipitation of the complex. The product was isolated by filtration, collected with a minimum of MeCN, and was purified by column chromatography on SiO_2 (MeCN/aq. 0.5 M $NaNO_3$ = 9: 1). After anion exchange, the product was obtained as a dark turquoise solid (45 mg, 56%).

^{1}H NMR (400 MHz, CD_3CN): δ 9.01 (s, 2H, A3,5), 8.95 (d, 2H, ^3J = 8.0 Hz, C3), 8.91 (d, 2H, ^3J = 8.0 Hz, D3), 8.90 (d, 2H, ^3J = 8.0 Hz, F3,5), 8.63 (d, 2H, ^3J = 8.0 Hz, E3), 8.59 (t, 1H, ^3J = 8.0 Hz, F4), 8.40 (d, 2H, ^3J = 8.0 Hz, B3), 8.06 (dd, 2H, ^3J = 8.0 Hz, ^3J = 7.6 Hz, E4), 7.89 (dd, 2H, ^3J = 8.0 Hz, ^3J = 7.6 Hz, D4), 7.74−7.84 (m, 6H, B4 + C4 + E6), 7.70 (d, 2H, ^3J = 6.0 Hz, D6), 7.60 (d, 2H, ^3J = 5.6 Hz, C6), 7.30−7.40 (m, 6H, B6 + D5 + E5), 7.23 (dd, 2H, ^3J = 7.6 Hz, ^3J = 6.0 Hz, C5), 6.88 (dd, 2H, ^3J = 7.6 Hz, ^3J = 5.6 Hz, B5), 4.12 (s, 3H, CO_2CH_3).

^{13}C NMR (100 MHz, CD_3CN): δ 227.4, 168.8, 168.3, 158.7, 156.9, 156.8, 156.2, 156.1, 154.7, 154.3, 154.1, 148.8, 147.4, 142.3, 139.7, 138.6, 138.3, 138.1, 136.4, 129.8, 129.7, 129.6, 129.3, 128.8, 125.8, 125.5, 125.5, 125.3, 123.6, 121.6, 52.8.

Anal. Calcd for $C_{57}H_{40}F_{18}N_{11}O_2P_3Ru_2 \cdot 3H_2O$: C, 42.73; H, 2.89; N, 9.62. Found: C, 42.93; H, 2.85; N, 9.46.

MALDI-TOF-MS (DHB Matrix): m/z = 1114.12 [M$^+$] (calcd for $C_{57}H_{40}N_{11}O_2Ru_2$, 1114.15).

[(N^C^N)Ru)$_2$(μ-tppz)](PF$_6$)$_2$, [5a]$^{2+}$. A suspension of [($RuCl_3$)$_2$tppz] (46 mg, 0.057 mmol), N^C(H)^N (45 mg, 0.20 mmol), and 10 drops of *N*-methylmorpholine in ethylene glycol (25 mL) was heated to 150 °C using microwave radiation. Aqueous KPF_6 was added to the green solution upon which the product precipitated and was isolated by filtration. The product was purified by column chromatography on SiO_2 (MeCN/aq. 0.5 M $NaNO_3$ = 9:1). After anion exchange, the product was obtained as a green solid (43 mg, 56%).

^{1}H NMR (400 MHz, CD_3CN): δ 8.89 (d, 4H, ^3J = 8.0 Hz, C3), 8.41 (d, 4H, ^3J = 8.0 Hz, A3,5), 8.29 (d, 4H, ^3J = 8.0 Hz, B3), 7.77 (dd, 4H, ^3J = 8.0 Hz, ^3J = 8.0 Hz, B4), 7.71 (dd, 4H, ^3J = 8.0 Hz, ^3J = 7.6 Hz, C4), 7.62 (t, 2H, ^3J = 8.0 Hz, A4), 7.57 (d, 4H, ^3J = 5.2 Hz, C6), 7.43 (d, 4H, ^3J = 5.2 Hz, B6), 7.19 (dd, 4H, ^3J = 7.6 Hz, ^3J = 5.2 Hz, C5), 6.84 (dd, 4H, ^3J = 8.0 Hz, ^3J = 5.2 Hz, B5).

^{13}C NMR (100 MHz, CD_3CN): δ 219.6, 169.4, 158.1, 155.8, 153.9, 146.7, 142.4, 137.4, 135.6, 128.9, 128.3, 125.4, 122.9, 122.7, 120.9.

Anal. Calcd for $C_{56}H_{38}F_{12}N_{10}P_2Ru_2$: C, 50.08; H, 2.85; N, 10.43. Found: C, 49.86; H, 2.82; N, 10.31.

MALDI-TOF-MS (DHB Matrix): m/z = 1054.14 [M$^+$] (calcd for $C_{56}H_{38}N_{10}Ru_2$, 1054.14).

[(MeO$_2$C−N^C^N)Ru)$_2$(μ-tppz)](PF$_6$)$_2$, [5b]$^{2+}$. A solution of [**2b**](PF$_6$) (21 mg, 0.023 mmol) in DMF (6 mL) was added to [**6b**](PF$_6$) (38 mg, 0.057 mmol). The resulting solution was heated under reflux for 16 h. An excess of KPF_6 was added, and the solution poured into H_2O (80 mL), which resulted in the precipitation of the complex. The product was isolated by filtration, collected with a minimum of MeCN, and was purified by column chromatography on SiO_2 (MeCN/aq. 0.5 M $NaNO_3$ = 9:1). After anion exchange, the product was obtained as a dark green solid (30 mg, 87%).

^{1}H NMR (400 MHz, CD_3CN): δ 9.01 (s, 4H, A3,5), 8.89 (d, 4H, ^3J = 8.0 Hz, C3), 8.42 (d, 4H, ^3J = 8.0 Hz, B3), 7.82 (dd, 4H, ^3J = 8.0 Hz, ^3J = 7.6 Hz, B4), 7.72 (dd, 4H, ^3J = 8.0 Hz, ^3J = 7.6 Hz, C4), 7.54 (d, 4H, ^3J = 5.6 Hz, C6), 7.51 (d, 4H, ^3J = 5.6 Hz, B6), 7.17 (dd, 4H, ^3J = 7.6 Hz, ^3J = 5.6 Hz, C5), 6.91 (dd, 4H, ^3J = 7.6 Hz, ^3J = 5.6 Hz, B5), 4.13 (s, 6H, CO_2CH_3).

^{13}C NMR (100 MHz, CD_3CN): δ 229.4, 168.9, 168.5, 157.6, 156.0, 154.0, 146.2, 142.8, 137.7, 136.1, 129.1, 128.5, 125.3, 124.6, 123.5, 121.4, 52.7.

Anal. Calcd for $C_{60}H_{42}F_{12}N_{10}O_4P_2Ru_2$: C, 49.39; H, 2.90; N, 9.60. Found: C, 49.32; H, 2.95; N, 9.49.

MALDI-TOF-MS (DHB Matrix): m/z = 1170.14 [M$^+$] (calcd for $C_{60}H_{42}N_{11}O_4Ru_2$, 1170.15).

X-ray Crystal Structure Determination of [Ru(MeO$_2$C−N^C^N)(MeCN)$_3$](PF$_6$). [$C_{24}H_{22}N_5O_2Ru$](PF$_6$), FW = 658.51, orange needle, 0.42 × 0.18 × 0.09 mm^3, monoclinic, $P2_1/c$ (no. 14), a = 8.4400(4), b = 9.8278(6), c = 31.6273(18) Å, β = 102.389(2)°, V = 2562.3(2) Å^3, Z = 4, D_x = 1.707 g/cm^3, μ = 0.751 mm^{-1}. 21495 Reflections were measured on a Nonius Kappa CCD diffractometer with rotating anode (graphite monochromator, λ = 0.71073 Å) up to a resolution of $(\sin\theta/\lambda)_{max}$ = 0.59 Å^{-1} at a temperature of 150 K. There were several crystal fragments present and only the non-overlapping reflections of the major component were used. An absorption correction based on multiple measured reflections was applied[76] (0.55−0.94 correction range). 4464 Reflections were unique (R_{int} = 0.070). The structure was solved with automated Patterson Methods (DIRDIF-99[77]) and refined with SHELXL-97[78] against F^2 of all reflections. Non-hydrogen atoms were refined freely with anisotropic displacement parameters. Hydrogen atoms were introduced in calculated positions and refined with a riding model. 410 Parameters were refined with 414 restraints concerning the disordered PF_6 anion. *R1*/*wR2* [$I > 2\sigma(I)$]: 0.0599/0.1516. *R1*/*wR2* [all refl.]: 0.0813/0.1647. S = 1.130. Residual electron density between −1.23 and 2.43 e/Å^3. Geometry calculations and checking for higher symmetry was performed with the PLATON program.[79]

Acknowledgment. The authors gratefully acknowledge the support from the European Commission through the funding of the project FULLSPECTRUM within the Sixth Framework Program under number SES6-CT-2003-502620. This work was financially supported (M.L., A.L.S.) by the Council for Chemical Sciences of The Netherlands Organization for Scientific Research (CW-NWO). The work of RWAH is part of the research programme of the Stichting voor Fundamenteel Onderzoek der Materie (FOM), which is financially supported by the NWO. We acknowledge NWO/NCF for the supercomputer time on ASTER, SARA (The Netherlands, project number SG-032).

Supporting Information Available: X-ray crystal structure determination of [Ru(MeO$_2$C−N^C^N)(MeCN)$_3$](PF$_6$). NMR spectrum of [**4a**]$^{3+}$. Applied basis sets, optimized molecular geometries, energies, Mulliken populations, isodensity plots of the frontier molecular orbitals, and electronic transition of [**3**]$^{n+}$, [**4a**]$^{n+}$, [**4b**]$^{n+}$, [**5a**]$^{n+}$, and [**5b**]$^{n+}$. This material is available free of charge via the Internet at http://pubs.acs.org.

(76) Sheldrick, G. M. *SADABS: Area-Detector Absorption Correction*, v2.10; Universität Göttingen: Göttingen, Germany, 1999.

(77) Beurskens, P. T.; Admiraal, G.; Beurskens, G.; Bosman, W. P.; Garcia-Granda, S.; Gould, R. O.; Smits, J. M. M.; Smykalla, C. *The DIRDIF99 program system*, Technical Report of the Crystallography Laboratory at University of Nijmegen; University of Nijmegen: Nijmegen, The Netherlands, 1999.

(78) Sheldrick, G. M. *Acta Crystallogr. A* **2008**, *64*, 112–122.

(79) Spek, A. L. *J. Appl. Crystallogr.* **2003**, *36*, 7–13.